Atmos. Chem. Phys. Discuss., https://doi.org/10.5194/acp-2018-373
Manuscript under review for journal Atmos. Chem. Phys.
Discussion started: 26 April 2018

Atmospheric Chemistry and Physics Discussions

Characterization of Aerosol Composition, Aerosol Acidity and Organic Acid Partitioning at an Agriculture-Intensive Rural Southeastern U.S. Site

Theodora Nah,[1] Hongyu Guo,[1] Amy P. Sullivan,[2] Yunle Chen,[1] David J. Tanner,[1] Athanasios Nenes,[1,3,4,5] Armistead Russell,[6] Nga Lee Ng,[1,3] L. Gregory Huey[1] and Rodney J. Weber[1,*]

[1]*School of Earth and Atmospheric Sciences, Georgia Institute of Technology, Atlanta, GA, USA*
[2]*Department of Atmospheric Science, Colorado State University, Fort Collins, CO, USA*
[3]*School of Chemical and Biomolecular Engineering, Georgia Institute of Technology, Atlanta, GA, USA*
[4]*ICE-HT, Foundation for Research and Technology, Hellas, 26504 Patras, Greece*
[5]*IERSD, National Observatory of Athens, P. Penteli, 15236, Athens, Greece*
[6]*School of Civil and Environmental Engineering, Georgia Institute of Technology, Atlanta, GA, USA*

** To whom correspondence should be addressed: rweber@eas.gatech.edu*

Abstract

The implementation of stringent emission regulations has resulted in the decline of anthropogenic pollutants including sulfur dioxide (SO_2), nitrogen oxides (NO_x) and carbon monoxide (CO). In contrast, ammonia (NH_3) emissions are largely unregulated, with emissions projected to increase in the future. We present real-time aerosol and gas measurements from a field study conducted in an agricultural-intensive region in the southeastern U.S. during the fall of 2016 to investigate how NH_3 affects particle acidity and SOA formation via the gas-particle partitioning of semi-volatile organic acids. Particle water and pH were determined using the ISORROPIA-II thermodynamic model and validated by comparing predicted inorganic HNO_3-NO_3^- and NH_3-NH_4^+ gas-particle partitioning ratios with measured values. Our results showed that despite the high NH_3 concentrations (study average 8.1 ± 5.2 ppb), PM_1 were highly acidic with pH values ranging from 0.9 to 3.8, and a study-averaged pH of 2.2 ± 0.6. PM_1 pH varied by approximately 1.4 units diurnally. Formic and acetic acids were the most abundant gas-phase organic acids, and oxalate was the most abundant particle-phase water-soluble organic acid anion. Measured particle-phase water-soluble organic acids were on average 6 % of the total non-refractory PM_1 organic aerosol mass. The measured molar fraction of oxalic acid in the particle phase (i.e., particle-phase oxalic acid molar concentration divided by the total oxalic acid molar concentration) ranged between 47 and 90 % for PM_1 pH 1.2 to 3.4. The measured oxalic acid gas-particle partitioning ratios were in good agreement with their corresponding thermodynamic predictions, calculated based on oxalic acid's physicochemical properties, ambient temperature, particle water and pH. In contrast, gas-particle partitioning of formic and

Atmos. Chem. Phys. Discuss., https://doi.org/10.5194/acp-2018-373
Manuscript under review for journal Atmos. Chem. Phys.
Discussion started: 26 April 2018

acetic acids were not well predicted for reasons currently unknown. For this study, higher NH_3 concentrations relative to what has been measured in the region in previous studies had minor effects on PM_1 organic acids and their influence on the overall organic aerosol and PM_1 mass concentrations.

1. Introduction

Ammonia (NH_3) is the most abundant basic gas in the troposphere and plays an important role in many atmospheric processes. It is a major neutralizer of atmospheric acidic species, reacting readily with sulfuric acid (H_2SO_4) and nitric acid (HNO_3) to form ammonium sulfate and nitrate salts (e.g., $(NH_4)_2SO_4$, and other forms such as NH_4HSO_4, $(NH_4)_3H(SO_4)_2$, and NH_4NO_3), which are often the main inorganic components of atmospheric aerosols. Wet and dry deposition are the principle NH_3 sinks (Dentener and Crutzen, 1994). NH_3 is spatially heterogeneous, with the highest concentrations typically found near emission sources (Seinfeld and Pandis, 2016). The dominant NH_3 sources in rural areas are agricultural in nature, and include the application of fertilizers and volatilization of livestock waste (Reis et al., 2009; Ellis et al., 2013; Van Damme et al., 2014). Biomass burning, either from wildfires or from controlled burning during land-clearing operations, is also a significant source of NH_3 in rural environments. The primary source of NH_3 in urban areas are industrial emissions, though vehicular emissions can be a significant NH_3 source in some heavily populated cities (Reis et al., 2009; Yao et al., 2013; Sun et al., 2017).

In the US, implementation of stringent emission controls on traditional anthropogenic air pollutants, such as sulfur dioxide (SO_2), nitrogen oxides (NO_x) and carbon monoxide (CO), have led to steady decreases in their emissions, and consequently their concentrations (Blanchard et al., 2013a; Xing et al., 2013). In contrast, NH_3 emissions are largely unregulated, and are projected to increase due to increased agricultural operations to feed a growing world population (Reis et al., 2009; Ellis et al., 2013). Satellite observations showed that gas-phase NH_3 concentrations have increased substantially in US agricultural areas from 2002 to 2014 (Warner et al., 2017). More wildfires from a changing climate, or from controlled burning for land clearing for agricultural use, may also lead to increased NH_3 emissions (Reis et al., 2009; Pechony and Shindell, 2010; Warner et al., 2016). These trends suggest that NH_3 could play an increasingly important role in atmospheric chemistry.

Previous laboratory studies have shown that NH_3 can influence secondary organic aerosol (SOA) formation and processing. For example, NH_3 increases SOA mass yields in the α-pinene ozonolysis system, and is hypothesized to be due to the formation of ammonium salts from the reaction of NH_3 with organic acids (Na et al., 2007). The heterogeneous uptake of NH_3 by SOA can also lead to the formation of particulate organonitrogen compounds, a class of brown carbon species that can reduce visibility and impact climate (Laskin et al., 2010; Updyke et al., 2012; Lee et al., 2013; Laskin et al., 2015).

The southeastern U.S. is a natural outdoor laboratory for studying the effects of biogenic-anthropogenic interactions on atmospheric aerosol formation and processing. Subtropical vegetation composed mainly of mixed conifer and deciduous forests emit large quantities of biogenic volatile organic compounds (BVOCs) that can act as precursors for SOA formation (Blanchard et al., 2011; Guenther et al., 2012; Blanchard et al., 2013b). Large urban centers and small towns are surrounded by large expanses of forests and widespread rural areas with agricultural activities. Scattered within the southeastern U.S. are also coal-burning power plants and industrial facilities. Anthropogenic activities in this region emit large concentrations of VOCs, SO_2, NO_x, CO, NH_3 and aerosols (Blanchard et al., 2013c). Similar to other parts of the U.S., SO_2, CO and NO_x concentrations have decreased steadily in the southeastern U.S. due to the implementation of emission controls (Blanchard et al., 2013a). In contrast, gas-phase NH_3 concentrations have increased in the southeastern U.S. over the same time period (Saylor et al., 2015). These factors make the southeastern U.S. an intriguing place to study the influence of NH_3 on atmospheric aerosol chemistry.

We performed aerosol and gas measurements during a field study conducted in Yorkville, Georgia, U.S., in the fall of 2016, with the goal of understanding how NH_3 affects aerosol acidity and SOA formation. The field site is surrounded by forest and agricultural land, affording an opportunity to make ambient observations in an area impacted by local emissions of BVOCs and NH_3. In this paper, we present gas and aerosol composition measurements that includes a suite of organic acids. The thermodynamic equilibrium model, ISORROPIA-II, is used to calculate particle water and pH based on measured inorganic aerosol and gas composition (Nenes et al., 1998; Fountoukis and Nenes, 2007), and these predictions are compared to observed gas-particle partitioning of NH_3, HNO_3 and organic acids. Together, these measurements are used to

97 determine how aerosol acidity affects the mass concentration of particle-phase organic acids at
98 this site.

99 **2. Methods**

100 **2.1. Field site**

101 Aerosol and gas measurements were conducted at the Yorkville, Georgia (33.929 N,
102 85.046 W) SouthEastern Aerosol Research and Characterization (SEARCH) field site from mid-
103 August to mid-October 2016. This is one of the sampling sites for the Southeastern Center for
104 Air Pollution and Epidemiology (SCAPE) study where aerosol characterization measurements
105 were conducted in the summer and winter of 2012 (Xu et al., 2015a; Xu et al., 2015b). A detailed
106 description of the field site can be found in Hansen et al. (2003). This rural site is situated in a
107 mixed forest-agriculture area approximately 55 km northwest and generally upwind of Atlanta.
108 The immediate surrounding area is used for cattle grazing and poultry concentrated animal
109 feeding operations (CAFOs) (Fig. S1). There are no major roads near the field site and nearby
110 traffic emissions were negligible. A large coal-fired power plant (Plant Bowen) is situated
111 approximately 25 km north of the site. Hence, the field site is impacted mainly by BVOC and
112 NH_3 emissions, with occasional spikes in SO_2 and minimal influence from urban anthropogenic
113 pollutants such as HNO_3, O_3, NO_x and CO (Fig. S2). The sampling period was characterized by
114 moderate temperatures (24.0 °C average, 32.6 °C max, 9.5 °C min) and high relative humidities
115 (68.9 % RH average, 100 % RH max, 21.6 % RH min). Meteorological data are shown in Fig.
116 S3. Data reported are displayed in eastern daylight time (EDT).

117 **2.2. Instrumentation**

118 Instruments were housed in a temperature controlled (~20 °C) trailer during the field
119 study. Gas-phase HNO_3, SO_2 and organic acids (formic, acetic, oxalic, butyric, glycolic,
120 propionic, valeric, malonic and succinic acids) were measured by a custom-built chemical
121 ionization mass spectrometer (CIMS) using sulfur hexafluoride ions (SF_6^-) as reagent ions. SO_2
122 and HNO_3 were detected as fluoride adducts ($F_2SO_2^-$ and NO_3^-•HF, respectively) while the
123 organic acids (HX) were detected primarily as conjugated anions (X^-) by the quadrupole mass
124 spectrometer (Huey et al., 1995; Huey et al., 2004; Nah et al., 2018). This CIMS is referred
125 hereafter as the SF_6-CIMS. Gas-phase NH_3 was measured by an additional custom-built CIMS

using protonated ethanol clusters ($((C_2H_5OH)_n^+$) as reagent ions. NH_3 was detected primarily as NH_4^+ ions by the quadrupole mass spectrometer (Nowak et al., 2002; Yu and Lee, 2012; You et al., 2014a). This CIMS is referred hereafter as the NH_3-CIMS.

Since HNO_3, NH_3 and organic acids may condense on surfaces, both SF_6-CIMS and NH_3-CIMS used inlet configurations that minimized wall interactions (Huey et al., 2004; Nowak et al., 2006). Each CIMS was connected to an inlet (a 7.6 cm ID aluminum pipe) that protruded beyond the trailer's wall by ~40 cm into the ambient air. Both inlets were ~2 m above the ground. A donut-shaped ring was attached to the ambient sampling port of each pipe to curtail the influence of crosswinds on the pipe's flow dynamics. Both rings were wrapped with a fine wire mesh to prevent ingestion of insects. A flow of ~2800 L min^{-1} was maintained in each pipe using regenerative blowers (AMETEK Windjammer 116637-03). Part of this flow (7 L min^{-1} for the SF_6-CIMS and 4.6 L min^{-1} for the NH_3-CIMS) was sampled through a custom-made three-way PFA Teflon valve, which connected the pipe's center to the CIMS sampling orifice and could be switched automatically between ambient and background measurements.

Background measurements were performed every 25 min for 4 min for both the SF_6-CIMS and NH_3-CIMS. During each background measurement, the sampled air flow was passed through an activated charcoal scrubber (Sigma Aldrich) that removed SO_2, HNO_3 and organic acids prior to delivery into the SF_6-CIMS, and through a silicon phosphate scrubber (Perma Pure Inc.) that removed NH_3 prior to delivery into the NH_3-CIMS. > 99 % of the targeted species were removed during background measurements for both the SF_6-CIMS and NH_3-CIMS. Standard addition calibrations were performed every 5 h for the SF_6-CIMS using the outputs of a 1.12 ppm $^{34}SO_2$ gas cylinder (Scott-Marrin Inc.) and a formic or acetic acid permeation device (VICI Metronics). Calibrations for the other gases measured by the SF_6-CIMS were performed in post-field laboratory work, details of which can be found in Nah et al. (2018) and SI section S1. Standard addition calibrations were performed hourly for the NH_3-CIMS using the output of a NH_3 permeation device (KIN-TEK). The outputs of the formic and acetic acid permeation devices were measured periodically by scrubbing the output of the permeation tube in deionized water, followed by ion chromatography analysis for formate and acetate. The emission rate of the NH_3 permeation device was measured using UV optical absorption (Neuman et al., 2003).

The detection limits for species measured by the SF_6-CIMS and NH_3-CIMS were approximated from 3 times the standard deviation values (3σ) of the ion signals measured during background mode. The detection limits for HNO_3, SO_2 and the various organic acids measured by the SF_6-CIMS ranged from 1 to 60 ppt for 2.5 min integration periods, which corresponded to the length of a background measurement with a 0.04 s duty cycle for each *m/z* (Table S1). Measurement uncertainties for the concentrations of HNO_3, SO_2 and the various organic acids originate mainly from calibration measurements, and were between 12 and 25 % (Table S1). The detection limit for NH_3 measured by the NH_3-CIMS was 1 ppb for 2.3 min integration periods, which corresponded to the length of a background measurement with a 0.29 s duty cycle for the NH_4^+ ion. Measurement uncertainties for NH_3 concentrations were 13 %.

A high-resolution time-of-flight aerosol mass spectrometer (HR-ToF-AMS, Aerodyne Research Inc.) was used to measure the elemental composition of ambient non-refractory PM_1 (particles with aerodynamic diameters < 1 μm). Ambient air was sampled at 16.7 L min^{-1} though a URG PM_1 cyclone and then through a nafion dryer prior to delivery into the HR-ToF-AMS. Aerosols were dried to RH < 20 % to eliminate the influence of RH on the HR-ToF-AMS's particle collection efficiency. A detailed description of the HR-ToF-AMS can be found in the literature (DeCarlo et al., 2006; Canagaratna et al., 2007; Canagaratna et al., 2015). Briefly, the aerodynamic lens of the HR-ToF-AMS focused the dried submicron aerosols into a narrow beam. The aerosols were then impacted onto a heated tungsten surface (~600 °C) where they were flash vaporized. The resulting vapors were ionized by electron impact ionization (70 eV), and the ions were detected by a time-of-flight mass spectrometer. Gas-phase interferences were accounted for by subtracting the signals obtained during daily measurements of filtered, particle-free sampling air. Ionization efficiency calibrations were performed weekly using 300 nm ammonium nitrate and ammonium sulfate particles. Composition-dependent collection efficiencies were applied to the data using the procedure detailed by Middlebrook et al. (2012). Uncertainties in HR-ToF-AMS measurements were estimated to be approximately 25 % (Canagaratna et al., 2007).

Particle-phase water-soluble organic acids, inorganic cations and anions were measured using two Particle-into-Liquid Sampler (PILS) systems coupled to ion chromatographs (ICs) (Orsini et al., 2003). Each PILS sampled ambient air at nominally 16.7 L min^{-1} through a URG

185 PM_1 cyclone. Before PILS1, which was used to measure water-soluble inorganic cation and
186 anions, two long (24 cm) URG glass annular denuders coated with sodium carbonate and
187 phosphorous acid were used to remove acidic and basic gases. Before PILS2, which measured
188 water-soluble organic acids, a 28 cm parallel plate carbon denuder (Sunset Lab) was used to
189 remove organic gases (Eatough et al., 1993). In each PILS, aerosols were mixed with water
190 vapor at ~100 °C generated from heated ultrapure deionized water (Weber et al., 2001; Orsini et
191 al., 2003). The resulting droplets were impacted onto a plate, with the resulting liquid sample
192 analyzed by ICs. Each IC system was calibrated at the beginning and end of the study using five
193 multi-compound standards in order to create calibration curves. Periodically, a HEPA filter (Pall
194 Life Sciences) was placed on the inlet to determine the background in near real-time. The
195 measurement uncertainty for each IC system was about 10 %.

196 PILS1 was connected to two Dionex ICS-1500 ICs (Thermo Fisher Scientific) to measure
197 the water-soluble inorganic ions. These two IC systems include an isocratic pump, self-
198 regenerating anion or cation suppressor, and conductivity detector. This system will be referred
199 hereafter as the PILS-IC. Anions were separated using a Dionex IonPac AS15 guard and
200 analytical column (4 x 250 mm, Thermo Fisher Scientific) employing an eluent of 38 mM
201 sodium hydroxide at a flow rate of 1.5 mL min^{-1}. Cations were separated using a Dionex IonPac
202 CS12A guard and analytical column (4 x 250 mm, Thermo Fisher Scientific) employing an
203 eluent of 18 mM methanesulfonic acid at a flow rate of 1 mL min^{-1}. A new chromatogram was
204 obtained every 30 min with a sample loop fill time (i.e., ambient sample integration time) of 20
205 min. The limit of detection for the various anions and cations was approximately 0.01 μg m^{-3}.

206 PILS2 was coupled to a Dionex ICS-4000 capillary high-pressure ion chromatography
207 (HPIC) system to measure the water-soluble organic acids. The HPIC includes an eluent
208 generator, isocratic pump, degausser, suppressor, carbonate removal device, and conductivity
209 detector. This system will be referred hereafter as the PILS-HPIC. The organic acids were
210 separated using a Dionex AS11-HC-4μm capillary guard and analytical column (0.4 x 250mm,
211 Thermo Fisher Scientific), which used a potassium hydroxide gradient separation method at a
212 flow rate of 0.015 mL min^{-1}. A new chromatogram was obtained every 60 min with a sample
213 loop fill time of 2 min. The limit of detection for the various organic acids was approximately
214 0.001 μg m^{-3}.

Particle- and gas-phase water-soluble organic carbon ($WSOC_p$ and $WSOC_g$, respectively) were measured using two Sievers 900 series total organic carbon (TOC) analyzers (GE Analytical Instruments), as described by Sullivan et al. (2004). For $WSOC_p$ measurements, ambient air was sampled at 15.2 L min^{-1} through a URG PM_1 cyclone and a parallel plate carbon denuder into a PILS coupled to the first TOC analyzer. For $WSOC_g$ measurements, ambient air was sampled at 20 L min^{-1} through a Teflon filter (45 mm diameter, 2.0 μm pore size, Pall Life Sciences) to remove particles in the air stream. This filter was changed every 3 to 4 days. The particle-free air was then directed to a MIST chamber filled with ultrapure deionized water, which scrubbed the soluble gases at an air flow rate of 20 L min^{-1}. Soluble gases with Henry's law constants greater than 10^3 mole L^{-1} atm^{-1} were scrubbed into deionized water in the MIST chamber (Spaulding et al., 2002). The resulting MIST chamber liquid sample was analyzed by the second TOC analyzer. The TOC analyzers converted the organic carbon in the liquid samples to carbon dioxide using UV radiation and chemical oxidation. The carbon dioxide formed was then measured by conductivity. The amount of organic carbon in the liquid samples is proportional to the measured increase in conductivity of the dissolved carbon dioxide. Each $WSOC_p$ and $WSOC_g$ measurement lasted 4 min. Background $WSOC_p$ and $WSOC_g$ measurements were performed for 45 min every 12 h by stopping the sample air flow and rinsing the system with deionized water. Both TOC analyzers were calibrated at the beginning and end of the study using varying concentrations of sucrose solutions to create calibration curves (as specified by the instrument manual). The limit of detections for $WSOC_p$ and $WSOC_g$ were 0.2 and 0.4 μgC m^{-3}, respectively. The measurement uncertainties for $WSOC_p$ and $WSOC_g$ were estimated to be 10 % based on uncertainties in the TOC analyzer, sample air and liquid flows.

A suite of instruments operated by the SEARCH network provided supporting gas and aerosol measurements (Hansen et al., 2003; Edgerton et al., 2005, 2006). O_3 was measured by a UV absorption instrument (Thermo Fisher Scientific) with a temporal resolution of 1 min. NO and NO_x were measured by a chemiluminescence instrument (Thermo Fisher Scientific) with a temporal resolution of 1 min. NO_2 was obtained from the difference between NO and NO_x. CO was measured by a non-dispersive infrared absorption instrument (Thermo Fisher Scientific) with a temporal resolution of 1 min. NH_3 was measured by a denuder-based instrument (ARA) with a temporal resolution of 5 min. Comparisons of measurements by the NH_3-CIMS and denuder-based instrument will be presented in section 3.1. A filter-based particle composition

Atmos. Chem. Phys. Discuss., https://doi.org/10.5194/acp-2018-373
Manuscript under review for journal Atmos. Chem. Phys.
Discussion started: 26 April 2018

Atmospheric Chemistry and Physics Discussions

monitor (ARA) provided 24 h-integrated $PM_{2.5}$ measurements of particle mass and major inorganic ions measured offline by ion chromatography. Organic carbon (OC) and elemental carbon (EC) in $PM_{2.5}$ were measured by a OCEC Analyzer (Sunset Labs) with a temporal resolution of 1 h. This analyzer determined OC by thermal optical transmittance. VOCs were measured by a gas chromatography-flame ionization detector (GC-FID, Agilent Technologies) with a temporal resolution of 1h.

2.2. Particle pH and water calculation

The thermodynamic equilibrium model ISORROPIA-II was used to determine the phase state and composition of an NH_4^+-SO_4^{2-}-NO_3^--Cl^--Na^+-Ca^{2+}-K^+-Mg^{2+}-water inorganic aerosol in equilibrium with its corresponding gas-phase species (Fountoukis and Nenes, 2007; Nenes et al., 1998). This approach was used in previous studies to determine particle water and pH in different parts of the world (Guo et al., 2015; Bougiatioti et al., 2016; Guo et al., 2016; Weber et al., 2016; Guo et al., 2017a; Guo et al., 2017c; Shi et al., 2017). pH is defined as the negative logarithm of the hydronium ion (H_3O^+) activity in an aqueous solution. For simplicity, H_3O^+ is denoted here as H^+ even though we recognize that the unhydrated hydrogen ion is rare in aqueous solutions. The particle pH is calculated as:

$$pH = -\log_{10}\gamma_{H^+}H^+_{aq} = -\log_{10}\frac{1000\gamma_{H^+}H^+_{air}}{W_i + W_o} \cong -\log_{10}\frac{1000\gamma_{H^+}H^+_{air}}{W_i} \qquad (1)$$

where γ_{H^+} is the hydronium ion activity coefficient (assumed to be 1), H^+_{aq} (mole L^{-1}) is the molar concentration of hydronium ions in particle water (i.e., pH is defined in terms of molarity), H^+_{air} (μg m^{-3}) is the hydronium ion concentration per volume of air, and W_i and W_o (μg m^{-3}) are the bulk particle water concentrations associated with inorganic and organic species, respectively. In equation 1, the molecular weight of H^+ is taken as 1 g $mole^{-1}$, and 1000 is the factor needed for unit conversion of g L^{-1} to μg m^{-3}. H^+_{air} and W_i are outputs of the ISORROPIA-II model. Previous studies have shown that particle pH values predicted using only W_i are reasonably accurate since the sensitivity of particle pH to the effects of W_o is small (Guo et al., 2015). For the southeastern U.S., Guo et al. (2015) reported that particle pH values predicted using only W_i were systematically 0.15 to 0.23 units lower than those predicted using W_i + W_o during the 2013 Southern Oxidant Aerosol Study (SOAS) and SCAPE campaigns. Given this

small deviation and that organic aerosol hygroscopicity was not measured in this field study, we report particle pH only considering W_i.

ISORROPIA-II was run in "forward" mode, which assumes that aerosols are "metastable" with no solid precipitates, to predict particle pH and the partitioning of semi-volatile compounds. In "forward" mode, the model calculates the gas-particle equilibrium partitioning concentrations based on the input of the total concentration of a species (i.e., gas + particle). In "reverse" mode, the model calculates the gas-particle equilibrium partitioning concentrations based on the input of only the particle-phase concentration of a species. We used "forward" mode because the "reverse" mode is sensitive to measurement errors, which often result in large model biases in the predicted particle pH (Hennigan et al., 2015). The measured particle-phase inorganic NH_4^+, SO_4^{2-} and NO_3^- concentrations and gas-phase HNO_3 and NH_3 concentrations were used as model inputs. The "metastable" assumption is reasonable since the high RH (average RH 68.9 %) observed during the study indicated that the aerosols had likely deliquesced. We excluded data for periods where the RH was above 95 % since the exponential growth in particle liquid water with RH introduces large pH uncertainties (Malm and Day, 2001; Guo et al., 2015).

In using ISORROPIA-II to predict particle pH and the partitioning of semi-volatile compounds, we also assumed that the aerosols are internally mixed and that the particle pH does not change with particle size (i.e., the overall particle pH is characterized by the particle's bulk properties). As long as some small fraction of sulfate is mixed with various aerosol components, (e.g., non-volatile cations), the assumption that aerosols are completely internally mixed has a small effect on the predicted pH (Guo et al., 2017b). However, the presence of multiple organic and inorganic species in ambient aerosols may lead to multiple phases within the particle (i.e., phase separation). Consequently, this may result in the unequal distribution of inorganic species among different phases, each with its own water activity and inorganic concentration. Previous studies have shown that liquid-liquid and solid-liquid phase separations may occur for mixed organic and inorganic aerosols at low RH and organic aerosol oxygen-to-carbon atomic ratios (O/C) (Bertram et al., 2011; Song et al., 2012; You et al., 2013; You et al., 2014b; You and Bertram, 2015). Phase separations were always observed at O/C $\leq$ 0.5, while no phase separation was observed at O/C $\geq$ 0.8. The probability for the occurrence of phase separation decreased at

higher RH for 0.5 < O/C < 0.8. The average O/C for this field study is 0.69 ± 0.06. Organic acids were not included in the calculation of particle pH. This is reasonable since their total mass concentration was small compared to the total inorganic mass concentration. The study-averaged ratio of the organic acid mass concentration to the inorganic mass concentration is 0.25. Furthermore, Song et al. (2018) showed that including organic acid mass concentrations in thermodynamic model calculations had minor effects on particle pH if the system is in equilibrium. The validity of these assumptions and the resulting thermodynamic model predictions will be evaluated by comparing the predicted gas-particle partitioning ratios of semi-volatile inorganic compounds with measured values in section 3.3.

3. Results and Discussion

3.1. NH_3 observations

Continuous measurements of NH_3 were made using the NH_3-CIMS from 13 September to 12 October. Figures 1a and 1b show the time series and study-averaged diurnal profile of NH_3, respectively. NH_3 concentrations ranged from 0.7 to 39.0 ppb (0.5 to 28.5 μg m^{-3}), and exhibited consistent diurnal cycles. NH_3 was generally higher in the late mornings and early afternoons. Concentrations started to increase at 07:30, which coincided with an increase in temperature at sunrise (Fig. S3). Possible reasons for the morning increase include volatilization of particulate ammonium and animal waste, entrainment from the residual layer where NH_3 may not have been depleted, evaporation of dew or fog that contained dissolved NH_3, and emission from plant stomata (Ellis et al., 2011). NH_3 decreased at 14:30, approximately 1 hour before temperature decreased, and may be due to changes in the boundary layer height. The diurnal plot does not account for dilution as the boundary layer expanded, and only indicates that if emissions were solely from the surface and lower concentrations aloft, these NH_3 sources were of significant magnitude.

The average NH_3 concentration measured by the NH_3-CIMS is 8.1 ± 5.2 ppb. This is approximately 2 times higher than the average NH_3 concentration (3.8 ± 2.9 ppb) measured by the denuder-based instrument operated by the SEARCH network over the same time period (Fig. S4). Differences in NH_3 concentrations measured by the two instruments may be due to positive and negative sampling artifacts caused by differences in sampling inlets (e.g., inlet length and

location), frequency of calibration and background measurements, and (in the case of the denuder-based instrument) possible sample contamination during chemical analysis. Discussions on how differences in measured NH_3 concentrations affect PM_1 pH predictions will be presented in section 3.3. Nevertheless, there is a record of NH_3 concentrations measured by the denuder-based instrument at this site since 2008. Just prior to, and during this study, NH_3 concentrations are generally the highest observed since 2011 (Fig. S5). These elevated NH_3 concentrations may be due to sporadic biomass burning episodes caused by elevated temperatures and widespread drought across the southeastern U.S. in 2016 (Park Williams et al., 2017; Case and Zavodsky, 2018).

The NH_3-CIMS measurements are examined with the meteorological data to gain insights on the primary NH_3 sources during the sampling period. To account for wind speed, the 1-hour averaged NH_3 concentrations are first multiplied by their corresponding 1-hour averaged wind speeds. These normalized NH_3 concentrations are then used to construct a wind direction polar plot showing the average normalized NH_3 concentration per 10 degrees bin (Fig. 1c). The wind direction polar plot shows that the normalized NH_3 is approximately 2 times greater than the average when air masses are transported from the south-east, the general direction of the poultry CAFOs located approximately 2 km from the field site (Fig. S1), which are known for high NH_3 emissions. This conclusion is reaffirmed by NH_3 measurements by the SEARCH network's denuder-based instrument.

NH_3 concentrations measured by the two instruments in this study are substantially higher than those measured in three recent field studies conducted in the continental U.S.: 2010 California Nexus (CalNex) study, 2013 Southeast Nexus (SENEX) study and 2013 SOAS study (see Table 1). The differences in NH_3 may be attributed to differences in land use, proximity to CAFOs and meteorological conditions. The high NH_3 concentrations in this study allow us to make ambient observations of the effect of NH_3 on particle acidity and the gas-particle partitioning of semi-volatile inorganic and organic compounds, and compare them with previous studies.

3.2. PM_1 composition

The aerosol inorganic chemical composition was measured by several instruments during

this study. The HR-ToF-AMS, PILS-IC and PILS-HPIC measured the composition of PM_1, while a filter-based particle composition monitor measured the composition of $PM_{2.5}$. Comparisons of aerosol SO_4^{2-}, NO_3^- and NH_4^+ mass concentrations measured by these four instruments are summarized in Fig. S6. NH_4^+ measurements by the PILS-IC are not available for comparison due to denuder breakthrough that occurred during the study.

SO_4^{2-} measurements by the various instruments are generally well correlated with each other, with R^2 values ranging from 0.64 to 0.92. Although PM_1 SO_4^{2-} measurements by the two PILS systems show good agreement with each other, HR-ToF-AMS SO_4^{2-} measurements are approximately two times higher than the PILS and filter measurements. Similar systematic differences are also observed for NO_3^- and NH_4^+ measurements. NO_3^- and NH_4^+ measurements by the four instruments are moderately correlated (R^2 = 0.54 to 0.79 and R^2 = 0.94, respectively). NO_3^- measurements by the PILS and filter systems are mostly similar; however, HR-ToF-AMS PM_1 NO_3^- and NH_4^+ measurements are approximately three times and two times higher than the PILS and filter measurements. Although the higher HR-ToF-AMS PM_1 NO_3^- measurements may be due, in part, to the HR-ToF-AMS not being able to readily discriminate between the inorganic and organic nitrates, reasons for the HR-ToF-AMS PM_1 SO_4^{2-} and NH_4^+ measurements being systematically higher than the PILS and filter measurements are not known.

We estimated HR-ToF-AMS PM_1 mass concentrations that would be consistent with PILS and filter measurements by multiplying all the raw HR-ToF-AMS data by a constant factor of 0.5 (i.e., average of the PILS-HPIC/HR-ToF-AMS and PILS-IC/HR-ToF-AMS SO_4^{2-} slopes). The scaled HR-ToF-AMS data is used in all our subsequent analyses.

Figure 2 shows the time series and study-averaged diurnal profiles of non-refractory PM_1 species. The study-averaged non-refractory PM_1 organics, SO_4^{2-}, NO_3^- and NH_4^+ mass concentrations are 5.0 ± 2.3, 1.6 ± 0.4, 0.2 ± 0.1 and 0.4 ± 0.2 μg m^{-3}, respectively. Organics are the dominant non-refractory PM_1 species, accounting for 74.2 ± 7.9 % of the non-refractory PM_1 mass concentration during the field study. Organic aerosol mass concentration was slightly higher at night, which is likely caused by changes in the boundary layer height, emission sources and SOA formation processes (Xu et al., 2015b). Apportionment of organic aerosol sources will be discussed in an upcoming publication. SO_4^{2-} is the second most abundant non-refractory PM_1 species (16.3 ± 5.7 % mass fraction), followed by NH_4^+ (5.9 ± 2 % mass fraction) and NO_3^- (3.6

± 2.2 % mass fraction). SO_4^{2-} mass concentration peaked in the afternoon due to enhanced SO_2 photooxidation (Weber et al., 2003). The NO_3^- mass concentration measured by the HR-ToF-AMS is the nitrate functional group ($-ONO_2$) present on organic and inorganic nitrates. Hence, the diurnal profile of the NO_3^- mass concentration in Fig. 2 has contributions from both organic and inorganic nitrates. The NO_3^- mass concentration increased after sunset and peaked at sunrise due to the formation of organic nitrates from nighttime NO_3 chemistry and increased gas-to-particle partitioning of organic and inorganic nitrates as temperature decreased (Xu et al., 2015a; Xu et al., 2015b). Quantification of organic nitrates based on HR-ToF-AMS and PILS-IC PM_1 NO_3^- measurements will be discussed in a future publication. NH_4^+ mass concentration has moderate diurnal variations with marginally higher concentrations in the afternoon, likely due to the contrasting day/night phases of ammonium sulfate and ammonium nitrate formation. SO_4^{2-}, NO_3^- and NH_4^+ molar concentrations indicated that NH_4^+ is mainly associated with SO_4^{2-} in PM_1.

3.3. PM_1 pH predictions

CIMS HNO_3 and NH_3 data, scaled HR-ToF-AMS PM_1 SO_4^{2-} and NH_4^+ data, PILS-IC PM_1 NO_3^- and non-volatile cation (Cl^-, Na^+, Ca^{2+}, K^+ and Mg^{2+}) data, temperature and RH are used as ISORROPIA-II model inputs to predict PM_1 W_i and pH from 13 September to 6 October. Figure 3 shows the time series and study-averaged diurnal profiles of ISORROPIA-predicted PM_1 W_i and pH. PM_1 are highly acidic with pH values ranging from 0.9 to 3.8, and a study-averaged pH of 2.2 ± 0.6. The average PM_1 pH was 2.5 ± 0.6 during periods where the NH_3 concentration was higher than 13.3 ppb (i.e., study-averaged NH_3 concentration + 1 standard deviation = 8.1 + 5.2 = 13.3 ppb). The PM_1 pH values in this study are generally similar to those reported by Guo et al. (2015) at the same field site during winter 2012. Our observation that PM_1 are acidic despite the high NH_3 concentrations in this study is consistent with previous studies showing that particle pH has weak sensitivities to wide NH_3 and SO_4^{2-} mass concentration ranges due to pH buffering caused by the partitioning of NH_3 between the gas and particle phases (Weber et al., 2016; Guo et al., 2017c). This weak particle pH sensitivity also explains the small changes in PM_1 pH values (about 10 % lower, Fig. S7) when NH_3 measurements by the SEARCH network denuder-based instrument are used in ISORROPIA-II calculations (instead of NH_3-CIMS measurements).

Atmos. Chem. Phys. Discuss., https://doi.org/10.5194/acp-2018-373
Manuscript under review for journal Atmos. Chem. Phys.
Discussion started: 26 April 2018

PM_1 pH varied by approximately 1.4 units throughout the day. W_i has a study-averaged value of 1.6 ± 1.7 μg m^{-3}. PM_1 W_i and pH showed similar diurnal profiles, with both peaking in the mid-morning and reaching their minima in the mid-afternoon. These diurnal trends are consistent with those previously reported by Guo et al. (2015) for PM_1 measured during the summer and winter in different parts of the southeastern U.S., and reaffirm that diurnal variation in particle pH is driven by W_i and not aerosol chemistry.

The average PM_1 pH for this study is about 1 unit higher than those for the SENEX and SOAS campaigns (Table 1), and is likely due to the much higher abundance of NH_3 in this study. The average NH_3 mass concentration in this study is approximately 49 times and 15 times higher than those in the SENEX and SOAS campaigns, respectively. The average PM_1 pH for this study is similar to that for the CalNex campaign even though the average NH_3 mass concentration in this study is only approximately 4 times higher than that in the CalNex campaign (Guo et al., 2017a). This can be explained by PM_1 SO_4^{2-} and NO_3^- mass concentrations at CalNex being approximately 2 times and 18 times larger than those of this study, respectively. Aerosol inorganic SO_4^{2-} and NO_3^- species are highly hygroscopic. The much higher NO_3^- mass concentrations in the CalNex campaign (due, in part, to high NO_x emissions) increased particle W_i substantially, which diluted H^+ and raised particle pH, resulting in more gas-to-particle partitioning of NO_3^-, and eventually leading to pH levels similar to those observed in this study. This type of feedback does not happen in the southeastern U.S. where non-volatile SO_4^{2-} dominates the uptake of particle water.

The validity of this study's thermodynamic model predictions is evaluated by comparing the predicted gas-particle partitioning ratios of semi-volatile inorganic compounds (i.e., NO_3^- and NH_4^+) with measured values (Fig. S8). CIMS HNO_3 and NH_3 data, PILS-IC NO_3^- and scaled HR-ToF-AMS NH_4^+ data are used in this comparison. $\varepsilon(NO_3^-)$ and $\varepsilon(NH_4^+)$ are defined as the particle-phase molar concentration divided by the total molar concentration (gas + particle), i.e., $\varepsilon(NO_3^-) = NO_3^- / (HNO_3 + NO_3^-)$ and $\varepsilon(NH_4^+) = NH_4^+ / (NH_3 + NH_4^+)$. Predicted NH_3, NH_4^+ and $\varepsilon(NH_4^+)$ values are generally within 10 % of and are highly correlated (R^2 = 0.96 to 0.99) with measured values (Fig. S8). While predicted HNO_3 values generally agreed with measurements, substantial scatter can be seen between the predicted and measured values for NO_3^- and $\varepsilon(NO_3^-)$. This scatter can be attributed, at least in part, to uncertainties brought about by the low PM_1 NO_3^-

Atmos. Chem. Phys. Discuss., https://doi.org/10.5194/acp-2018-373
Manuscript under review for journal Atmos. Chem. Phys.
Discussion started: 26 April 2018

Atmospheric Chemistry and Physics Discussions

mass concentrations and effects of coarse mode cations (e.g., Na^+, Ca^{2+}, K^+ and Mg^{2+}) on fine mode HNO_3-NO_3^- gas-particle equilibrium (i.e., HNO_3 can partition to both fine and coarse modes, thereby affecting fine mode NO_3^- concentrations; no such effect occurs for NH_3-NH_4^+ gas-particle equilibrium). In general, the overall good agreement between model predictions and measurements indicated that our assumptions that aerosols are metastable (i.e., aerosols are supersaturated aqueous droplets) with no phase separation for the thermodynamic calculations are reasonable for the conditions of this study, and do not affect model predictions.

The molar fractions of NO_3^- and NH_4^+ in the particle phase (i.e., $\varepsilon(NO_3^-)$ and $\varepsilon(NH_4^+)$) measured in this study are compared with those measured during the CalNex, SENEX and SOAS campaigns. Figure 4 shows the measured $\varepsilon(NO_3^-)$ and $\varepsilon(NH_4^+)$ values as a function of their ISORROPIA-predicted particle pH for the various field studies. For each field study, only a subset of the data is chosen for this comparison ($1 \le W_i \le 4$ μg m^{-3} and 15 °C ≤ temperature ≤ 25 °C) to reduce the effects of variability of W_i and temperature on gas-particle partitioning for comparison with the calculated S (or sigmoidal) curves, which are calculated based on W_i = 2.5 μg m^{-3} and temperature = 20 °C. The S curves for HNO_3-NO_3^- and NH_3-NH_4^+ partitioning as a function of particle pH are also plotted as solid lines. The S curves are calculated based on the solubility and dissociation of NO_3^- and NH_4^+ species in water:

$$\varepsilon(NO_3^-) = \frac{H^*_{HNO_3} RTW_i \times 0.987 \times 10^{-14}}{\gamma_{H^+}\gamma_{NO_3^-} 10^{-pH} + H^*_{HNO_3} RTW_i \times 0.987 \times 10^{-14}} \quad (2)$$

$$\varepsilon(NH_4^+) = \frac{\frac{\gamma_{H^+} 10^{-pH}}{\gamma_{NH_4^+}} H^*_{NH_3} RTW_i \times 0.987 \times 10^{-14}}{1 + \frac{\gamma_{H^+} 10^{-pH}}{\gamma_{NH_4^+}} H^*_{NH_3} RTW_i \times 0.987 \times 10^{-14}} \quad (3)$$

where $H^*_{HNO_3}$ and $H^*_{NH_3}$ (mole^2 kg^{-2} atm^{-1}) are equilibrium constants and are the products of the Henry's law constant and the dissociation constant of HNO_3 and NH_3, respectively, R is the gas constant (8.314 m^3 Pa K^{-1} mol^{-1}), T is temperature (K), and γ_i's are activity coefficients. $H^*_{HNO_3}$ and $H^*_{NH_3}$ values at 20 °C are calculated using equations found in Clegg and Brimblecombe (1990) and Clegg et al. (1998), respectively. Activity coefficients predicted by ISORROPIA-II are $\gamma_{H^+-NO_3^-} = \sqrt{\gamma_{H^+}\gamma_{NO_3^-}} = 0.28$, $\gamma_{H^+} = 1$ and $\gamma_{NH_4^+} = 1$. Derivations of the analytically calculated S curves for $\varepsilon(NO_3^-)$ and $\varepsilon(NH_4^+)$ in equations 2 and 3 can be found in Guo et al.

(2017a). As shown in Fig. 4, the measured $\varepsilon(NO_3^-)$ and $\varepsilon(NH_4^+)$ values for the four field studies all generally converged on the calculated S curves. The higher particle pH values in this study and the CalNex campaign relative to those for the SENEX and SOAS campaigns resulted in less NH_3 and more HNO_3 partitioned to the particle phase, as predicted by these simple analytical expressions. A similar analysis will be performed for the organic acids in section 3.5.

3.4. WSOC and water-soluble organic acids

The time series and study-averaged diurnal profiles of $WSOC_g$ and $WSOC_p$ are shown in Fig. S9. The study-averaged $WSOC_g$ mass concentration (3.6 ± 2.7 μgC m^{-3}) is roughly four times higher than that of $WSOC_p$ (1.0 ± 0.6 μgC m^{-3}). The diurnal profile of $WSOC_p$ is somewhat flat, likely due to various organic aerosol sources having different water solubility and diurnal cycles, and compensating each other throughout the day (Xu et al., 2015b; Xu et al., 2017). In contrast, $WSOC_g$ displayed strong diurnal variations. $WSOC_g$ increased at 07:30, which coincided with the sharp increase in solar irradiance (Fig. S3). $WSOC_g$ decreased at 21:30, approximately 2 hours after sunset. Also shown in Fig. S9 are the time series and study-averaged diurnal profile of the mass fraction of total WSOC in the particle phase, i.e., $F_p = WSOC_p / (WSOC_p + WSOC_g)$. The peak F_p coincided with the minima of $WSOC_g$ at 07:30.

The study-averaged $WSOC_g$ and $WSOC_p$ (3.6 ± 2.7 μgC m^{-3} and 1.0 ± 0.6 μgC m^{-3}) are slightly lower than those measured during the SOAS campaign (SOAS $WSOC_g$ = 4.9 μgC m^{-3} and $WSOC_p$ = 1.7 μgC m^{-3}) (Xu et al., 2017). While the diurnal profiles of $WSOC_p$ in both studies are flat, the diurnal profiles of $WSOC_g$ measured in the two studies are different. $WSOC_g$ measured in the SOAS study decreased at sunset, while $WSOC_g$ measured in this study decreased 2 hours after sunset. Differences in $WSOC_g$ diurnal profiles in the two studies are likely due to differences in emission sources as a result of different sampling periods (SOAS was in early summer and this study was in early fall), land use and/or land cover. The ratio of $WSOC_p$ to OC for this study was estimated at 30 %, but this comparison is imprecise because $WSOC_p$ was PM_1 and OC was $PM_{2.5}$ (refer to Fig. S10 and SI section S2).

Figure 5 shows the time series of particle- and gas-phase concentrations of formic, acetic, oxalic, malonic, succinic, glutaric and maleic acids. Their diurnal profiles are shown in Fig. 6. Gas-phase measurements of glutaric and maleic acids are not available. Gas-phase measurements

503 of butyric, glycolic, propionic and valeric acids were also measured during the study and have
504 been presented in Nah et al. (2018), but will not be discussed here since their particle-phase
505 measurements are not available.

506 Assuming that all the measured organic acids are completely water-soluble, 30 % of the
507 $WSOC_g$ is comprised of these organic acids (Nah et al., 2018). Formic and acetic acids are the
508 most abundant gas-phase organic acids, with study averages of 2.2 ± 1.6 and 1.9 ± 1.3 μg m^{-3},
509 respectively. The study-averaged carbon mass fraction of $WSOC_g$ comprised of formic and
510 acetic acids are 7 and 13 %, respectively. All the gas-phase organic acids displayed strong and
511 consistent diurnal cycles, with higher concentrations being measured during warm and sunny
512 days. Their concentrations start to increase at sunrise (at 07:30), building to a peak between
513 15:30 and 19:30, then decrease overnight.

514 Nah et al. (2018) previously showed that the measured gas-phase organic acids during the
515 study, including oxalic acid, likely have the same or similar sources. Poor correlations between
516 gas-phase organic acid concentrations and those of anthropogenic pollutants (HNO_3, SO_2, CO
517 and O_3) indicated that these organic acids are not due to anthropogenic emissions, and are likely
518 biogenic in nature. Biogenic emissions of gas-phase organic acids and/or their BVOC precursors
519 are elevated at high temperatures, resulting in higher organic acid concentrations during warm
520 and sunny days. Some of these gas-phase organic acids may also be formed in the particle phase
521 during organic aerosol photochemical aging, with subsequent volatilization into the gas phase.

522 The measured particle-phase water-soluble organic acids contributed on average 6 % to
523 the scaled HR-ToF-AMS-measured organic aerosol mass concentration. The study-averaged
524 carbon mass fraction of $WSOC_p$ comprised of these organic acids is 4 %. Previous studies have
525 shown that particle-phase organic acids found in rural environments are oxidation products of
526 gas-phase aliphatic monocarboxylic acids, which are formed in the photochemical oxidation of
527 biogenic unsaturated fatty acids and other BVOC precursors (Kawamura and Gagosian, 1987;
528 Kawamura and Ikushima, 1993; Kerminen et al., 2000; Kawamura and Bikkina, 2016). These
529 particle-phase organic acids can also be produced during the multiphase photochemical aging of
530 ambient organic aerosols (Ervens et al., 2004; Lim et al., 2005; Sorooshian et al., 2007;
531 Sorooshian et al., 2010).

Oxalate is the most abundant measured particle-phase water-soluble organic acid anion (contributing a study-averaged 26 % to the total particle-phase organic acid mass concentration), with mass concentrations ranging from 0.01 to 0.34 μg m^{-3} and a study average of 0.07 ± 0.05 μg m^{-3}. Acetate (study average of 0.06 ± 0.03 μg m^{-3}) and formate (study average of 0.05 ± 0.03 μg m^{-3}) are the second and third most abundant measured particle-phase water-soluble organic acid anions, respectively. Particle-phase formate, acetate and maleate showed weak diurnal variations, and may be due, in part, to various emission sources having different diurnal cycles and compensating each other throughout the day. Particle-phase oxalate, malonate and succinate peaked in the mid- to late afternoon, while glutarate generally peaked in the mid-morning. This suggests that while the production of these organic acids is photochemically-driven, they likely have different BVOC precursors and/or different photochemical production pathways.

3.5. Gas-particle partitioning of organic acids

The online and simultaneous measurements of gas- and particle-phase organic acid mass concentrations provided the opportunity to study gas-particle partitioning behavior of semi-volatile organic compounds with respect to particle pH, as is more commonly done with semi-volatile inorganic species (see section 3.3). Since formic, acetic and oxalic acids are the three most abundant measured organic acids present in the gas and particle phases, we focus on the gas-particle partitioning behaviors of these three organic acids. The study-averaged molar fractions (± 1 standard deviation) of formic, acetic and oxalic acid in the particle phase (i.e., $\varepsilon(HCOO^-)$, $\varepsilon(CH_3CO_2^-)$ and $\varepsilon(C_2O_4^{2-})$) are 3.6 ± 3.6 %, 5.8 ± 5.0 % and 73.7 ± 9.8 %, respectively. The uncertainties of these ratios for formic, acetic and oxalic acids are 16, 16 and 17 %, respectively, which are obtained from the propagation of their SF_6-CIMS and PILS-HPIC measurement uncertainties.

3.5.1. Oxalic acid

To investigate the factors affecting oxalic acid gas-particle partitioning, the equation for the S curve describing the dependence of oxalic acid gas-particle partitioning (i.e., $\varepsilon(C_2O_4^{2-}) = C_2O_4^{2-} / (C_2H_2O_4 + C_2O_4^{2-})$) on particle pH is derived. As shown in SI section S3, the analytically calculated S curve for $\varepsilon(C_2O_4^{2-})$ can be simplified to:

$$\varepsilon(C_2O_4^{2-}) \cong \frac{H_{C_2H_2O_4} W_i RT\left(\frac{\gamma_H+\gamma_{C_2HO_4^-}}{\gamma_{C_2H_2O_4}}10^{-pH}+K_{a1}\right)\times 0.987\times 10^{-14}}{\gamma_{H^+}\gamma_{C_2HO_4^-}10^{-pH}+H_{C_2H_2O_4} W_i RT\left(\frac{\gamma_H+\gamma_{C_2HO_4^-}}{\gamma_{C_2H_2O_4}}10^{-pH}+K_{a1}\right)\times 0.987\times 10^{-14}} \quad (4)$$

where $H_{C_2H_2O_4}$ (mole L^{-1} atm^{-1}) is the Henry's law constant for oxalic acid, K_{a1} (mole L^{-1}) is the first acid dissociation constant for oxalic acid, R is the gas constant (8.314 m^3 Pa K^{-1} mol^{-1}), T is temperature (K), and γ_i's are activity coefficients. We used the web version of AIOMFAC (www.aiomfac.caltech.edu) (Zuend et al., 2008; Zuend et al., 2011; Zuend et al., 2012) to compute a study-averaged $\gamma_{C_2H_2O_4}$ value of 0.0492. Since AIOMFAC does not predict $\gamma_H+\gamma_{C_2HO_4^-}$, we assumed that $\gamma_H+\gamma_{C_2HO_4^-} = \gamma_H+\gamma_{NO_3^-}$, and used the ISORROPIA-predicted $\gamma_H+\gamma_{NO_3^-}$ value of 0.07. We used the average of $H_{C_2H_2O_4}$ values provided by Clegg et al. (1996), Compernolle and Muller (2014) and Saxena and Hildemann (1996) (6.11 x 10^8 mole L^{-1} atm^{-1} at 25 °C), and accounted for the effect of temperature using equation 19 in Sander (2015). Although K_{a1} also depends on temperature, we used the K_{a1} value at 25 °C (5.62 x 10^{-2} mole L^{-1}, (Haynes, 2014)) for all the oxalic acid S curve calculations since equations that compute K_{a1} values for pure aqueous oxalic acid solutions at different temperatures are not available in the literature. In addition, the temperatures observed in this study were close to 25 °C (study-average temperature = 23.4 ± 4.0 °C).

Different S curves for $\varepsilon(C_2O_4^{2-})$ are calculated using 1-hour average values obtained from the diurnal profiles of temperature and W_i (specifically at 00:30, 06:30 and 12:30). The shape of the S curve changes with the time of day due to the diurnal variations of temperature and W_i (Fig S11 and SI section S3). The S curves for $\varepsilon(C_2O_4^{2-})$ are very different from those of other acids, such as $\varepsilon(NO_3^-)$ (shown in Fig. 4b). From the S curves for $\varepsilon(C_2O_4^{2-})$, which are calculated using conditions in this study, some molar fraction of oxalic acid is always expected to be present in the particle phase, even at low particle pH (i.e., the S curve does not go to zero at low pH). In contrast, HNO_3 is expected to be present primarily in the gas phase at low particle pH (i.e., pH < 1) under similar temperature and W_i conditions. This is due primarily to differences in the Henry's law constants for the two acids. H_{HNO_3} (2.57 x 10^5 mole L^{-1} atm^{-1}) at 23.4 °C is three orders of magnitude smaller than $H_{C_2H_2O_4}$ (7.27 x 10^8 mole L^{-1} atm^{-1}) (Clegg and Brimblecombe, 1990; Sander, 2015). This means that some undissociated form of oxalate can be found in the

particle phase at any pH, and the molar fraction of this form increases with particle W_i (see Fig. S11). Oxalic acid's very high Henry's law constant combined with the W_i conditions in this study ensures that some fraction of the organic acid will be in the particle phase regardless the particle pH.

Figure 7 compares the measured $\varepsilon(C_2O_4^{2-})$ vs. ISORROPIA-predicted PM_1 pH to the analytically calculated S curves(s). The S curve is calculated based on the average temperature and W_i from 13 September to 6 October (23.4 ± 4.0 °C and 1.6 ± 1.7 μg m^{-3}, respectively). We also calculated the "upper" and "lower" bounds of this S curve based on one standard deviation from the average temperature and average W_i. Temperature = 27.4 °C and W_i = 0.5 μg m^{-3} are used for calculations of the "lower" bound, while temperature = 19.4 °C and W_i = 3.3 μg m^{-3} are used for calculations of the "upper" bound. For the ambient data, a range in W_i (0.5 to 4 μg m^{-3}) and temperature (15 to 31 °C) is chosen to be close to the analytical calculation. As shown in Fig. 7, the measured $\varepsilon(C_2O_4^{2-})$ generally converged around the S curve calculated using the average temperature and W_i values. Although there is some scatter, the measured ratios are mostly within the "upper" and "lower" bounds of the S curve.

We can also use the S curves for $\varepsilon(C_2O_4^{2-})$ in Fig. 7 to understand how high NH_3 events at the site affect oxalic acid gas-particle partitioning. Here we define high NH_3 events as periods where the NH_3 concentration was higher than 13.3 ppb (which is the study-averaged NH_3 concentration + 1 standard deviation). As discussed in section 3.3, the PM_1 pH during high NH_3 events is 2.5 ± 0.6, which is slightly higher than the study-averaged PM_1 pH of 2.2 ± 0.6. Based on the S curve calculated using the average temperature and W_i values, $\varepsilon(C_2O_4^{2-})$ increases from 81 % to 89 % when particle pH increases from 2.2 to 2.5. While this result indicates that high NH_3 concentrations can raise the particle pH sufficiently such that it can promote gas-to-particle partitioning of oxalic acid, this is not always the case. Specifically, increasing the particle pH from -2 (or lower) to 1 will not result in a significant increase in $\varepsilon(C_2O_4^{2-})$. Therefore, whether or not particle pH, and consequently oxalic acid gas-particle partitioning, is sensitive to NH_3 concentration depends strongly on particle pH values.

We also examined how well the analytically calculated S curve for $\varepsilon(C_2O_4^{2-})$ captures diurnal variations of the measured $\varepsilon(C_2O_4^{2-})$. The ambient data is divided into two 12 hour sets

(08:00 to 19:59 and 20:00 to 07:59) based on the diurnal profile of solar irradiance. Two S curves and their corresponding "upper" and "lower" bounds are calculated based on the average temperature and W_i of the two data sets, and are subsequently compared to the ambient data. As shown in Fig. S12, the measured $\varepsilon(C_2O_4^{2-})$ in both data sets are generally consistent with predicted values.

A number of inferences can be drawn from the overall good agreement between the predicted and measured molar fractions of oxalic acid in the particle phase in Figs. 7 and S11. Our assumptions regarding the activity coefficients, Henry's law constant and acid dissociation constants used in the S curve calculations of $\varepsilon(C_2O_4^{2-})$ are reasonable for the conditions of this study (or are at least self-consistent). S curves can be used to estimate activity coefficients based on gas-particle partitioning data in cases where they are not available in the literature if the other parameters are known. Analytically calculated S curves are a simple way of exploring how the gas-particle partitioning of semi-volatile inorganic and organic compounds in the atmosphere are affected by the compound's physicochemical properties (e.g., Henry's law constants and acid dissociation constants), temperature, W_i and pH. Overall, these results indicate that particle-phase oxalate is in equilibrium with gas-phase oxalic acid, and that particle pH can influence particle-phase oxalate concentrations. It also showed that particle-phase oxalate can be found over a broad pH range, and that the presence of oxalate does not necessarily provide insights of the particle pH. Because of its high Henry's law constant, particle-phase oxalate can be found in aerosols even at extremely low pH values (i.e., the flat region in Fig. 7), although our data cannot be used to test this since ambient particle pH values in this study are too high.

3.5.2 Formic and acetic acids

Similar comparisons between the predicted and measured $\varepsilon(HCOO^-)$ and $\varepsilon(CH_3CO_2^-)$ can also be made. Derivation of the equations for S curves describing the dependence of formic and acetic acid gas-particle partitioning (i.e., $\varepsilon(HCOO^-) = HCOO^- / (HCOOH + HCOO^-)$ and $\varepsilon(CH_3CO_2^-) = CH_3CO_2^- / (CH_3CO_2H + CH_3CO_2^-)$, respectively) on particle pH are similar to that of HNO_3 since they are monoprotic acids:

$$\varepsilon(HCOO^-) = \frac{H_{HCOOH} W_i RT\left(\frac{\gamma_H+\gamma_{HCOO^-}}{\gamma_{HCOOH}}10^{-pH}+K_{a1}\right)\times 0.987\times 10^{-14}}{\gamma_{H^+}\gamma_{HCOO^-}10^{-pH}+H_{HCOOH}W_i RT\left(\frac{\gamma_H+\gamma_{HCOO^-}}{\gamma_{HCOOH}}10^{-pH}+K_{a1}\right)\times 0.987\times 10^{-14}} \quad (5)$$

644 $$\varepsilon(CH_3CO_2^-) = \frac{H_{CH_3CO_2H} W_i RT \left(\frac{\gamma_H+\gamma_{CH_3CO_2^-}}{\gamma_{CH_3CO_2H}} 10^{-pH} + K_{a1}\right) \times 0.987 \times 10^{-14}}{\gamma_{H^+}\gamma_{CH_3CO_2^-} 10^{-pH} + H_{CH_3CO_2H} W_i RT \left(\frac{\gamma_H+\gamma_{CH_3CO_2^-}}{\gamma_{CH_3CO_2H}} 10^{-pH} + K_{a1}\right) \times 0.987 \times 10^{-14}} \quad (6)$$

645 where H_{HCOOH} and $H_{CH_3CO_2H}$ (mole L^{-1} atm^{-1}) are the Henry's law constants for formic and acetic
646 acid, K_{a1}'s (mole L^{-1}) are the first acid dissociation constants, R is the gas constant (8.314 m^3 Pa
647 K^{-1} mol^{-1}), T is temperature (K), and γ_i's are activity coefficients. We used the web version of
648 AIOMFAC (www.aiomfac.caltech.edu) (Zuend et al., 2008; Zuend et al., 2011; Zuend et al.,
649 2012) to compute study-averaged γ_{HCOOH} and γ_{CH_3COOH} values of 0.334 and 2.150, respectively.
650 Similar to the case of oxalic acid, we assumed that $\gamma_{H^+}\gamma_{HCOO^-} = \gamma_{H^+}\gamma_{CH_3COO^-} = \gamma_{H^+}\gamma_{NO_3^-}$, and
651 used the ISORROPIA-predicted $\gamma_{H^+}\gamma_{NO_3^-}$ value of 0.07. Temperature-dependent H_{HCOOH} and
652 $H_{CH_3CO_2H}$ values are obtained from Sander (2015) using the same methodology employed to
653 determine temperature-dependent $H_{C_2H_2O_4}$ values. We used K_{a1} values at 25 °C (1.78 x 10^{-4} mole
654 L^{-1} for formic acid, and 1.75 x 10^{-5} mole L^{-1} for acetic acid (Haynes, 2014)) for the S curve
655 calculations.

656 S curves for ε(HCOO$^-$) and ε($CH_3CO_2^-$) calculated based on temperature = 23.4 °C and
657 W_i = 1.6 μg m^{-3} can be seen in Fig. 8. Practically no formic or acetic acids are predicted to
658 partition to the particle phase (relative to oxalic acid) for the range of PM_1 pH calculated in this
659 study. This is due to significant differences in the Henry's law constants and acid dissociation
660 constants for the three organic acids. H_{HCOOH} and $H_{CH_3CO_2H}$ (9540 and 5370 mole L^{-1} atm^{-1},
661 respectively) at 23.4 °C are substantially smaller than $H_{C_2H_2O_4}$ (7.27 x 10^8 mole L^{-1} atm^{-1})
662 (Sander, 2015). The K_{a1} values for formic and acetic acids (1.78 x 10^{-4} and 1.75 x 10^{-5} mole L^{-1},
663 respectively) are also considerably smaller than the K_{a1} value for oxalic acid (5.62 x 10^{-2} mole L^{-1})
664 (Haynes, 2014). Note that H_{HNO_3} is between that of $H_{C_2H_2O_4}$ and those of H_{HCOOH} and
665 $H_{CH_3CO_2H}$ (compare Fig. 4b with Figs. 7 and 8).

666 As shown in Fig. 8, higher than expected levels of formate and acetate are observed in the
667 particle phase. This has also been reported in previous studies (Liu et al., 2012). Laboratory tests
668 showed that the disagreement cannot be explained by positive biases in the particle-phase
669 formate and acetate PILS-HPIC measurements resulting from less than 100 % gas removal by
670 the carbon denuder. The measured denuder efficiency for formic acid was ≥ 99.97% (SI section

671 S4). The possibility that formic and acetic acid dimers in the aqueous phase (Schrier et al., 1964;
672 Gilson et al., 1997; Chen et al., 2008) may result in higher than predicted molar fractions of
673 formate and acetate in the particle phase was explored, but also could not explain the observed
674 gas-particle partitioning of these acids (SI section S5). The disagreement could be due to
675 incorrect Henry's law constants for formic and acetic acids. However, the Henry's law constants
676 for formic and acetic acid would have to be ~10^4 times and ~3 x 10^5 times larger than their
677 literature values, respectively, in order for their S curves to match our measured molar fractions
678 of formic and acetic acid in the particle phase. More research is needed to explain this
679 disagreement.

680 **4. Summary**

681 Gas- and particle-phase measurements were conducted in Yorkville, Georgia (a rural
682 field site) during fall 2016. The goal of the field study was to understand how NH_3 affects
683 particle acidity, and consequently SOA formation through the gas-particle partitioning of semi-
684 volatile inorganic and organic compounds. Since it is a rural site surrounded by forest,
685 agricultural land and CAFOs, this study provided an opportunity for ambient observations in an
686 area impacted by high local emissions of BVOCs and NH_3.

687 NH_3 concentrations measured by the NH_3-CIMS ranged from 0.7 to 39.0 ppb (study
688 average 8.1 ± 5.2 ppb), which were substantially higher than typical levels in the southeastern
689 U.S.. PM_1 inorganic chemical composition, gas-phase HNO_3 and NH_3 concentrations,
690 temperature and RH were used as model inputs in the ISORROPIA-II thermodynamic model to
691 calculate PM_1 pH and W_i. PM_1 pH ranged from 0.9 to 3.8, with a study-averaged pH of 2.2 ±
692 0.6. The measured and predicted HNO_3-NO_3^- and NH_3-NH_4^+ gas-particle partitioning ratios were
693 in good agreement. The measured gas-phase organic acids were estimated to contribute 30 % of
694 the overall $WSOC_g$ on a carbon mass basis, whereas measured particle-phase organic acids
695 comprised 6 % of the total organic aerosol mass concentration and 4 % of the overall $WSOC_p$ on
696 a carbon mass basis. Formic and acetic acids were the most abundant gas-phase organic acids,
697 with study averages of 2.2 ± 1.6 and 1.9 ± 1.3 μg m^{-3}, respectively. Oxalate was the most
698 abundant particle-phase water-soluble organic acid anion, with a study average of 0.07 ± 0.05 μg
699 m^{-3}. Measured oxalic acid gas-particle partitioning ratios generally agreed with analytical
700 predictions, which were based on oxalic acid's physicochemical properties (specifically, its

Henry's law constants, acid dissociation constants and activity coefficients), temperature, W_i and particle pH. The partitioning of oxalic acid to the particle phase is highly sensitive to temperature and W_i. In contrast, the partitioning of formic and acetic acids to the particle phase were higher than predicted for reasons currently unknown.

Although past air regulations have resulted in decreased sulfate, nitrate and ammonium aerosol mass concentrations across the U.S., our study suggests that the current limited regulation of NH_3 emissions may result in some increase in the organic aerosol mass concentration due to increased gas-to-particle partitioning of some organic acids. However, in this study, the effect was small since the organic acids comprised a small fraction of the overall organic aerosol mass.

5. Acknowledgements

The authors thank Eric Edgerton (Atmospheric Research and Analysis, Inc.) for providing SEARCH network measurements and meteorological data.

6. Funding

This publication was developed under U.S. Environmental Protection Agency (EPA) STAR Grant R835882 awarded to Georgia Institute of Technology. It has not been formally reviewed by the EPA. The views expressed in this document are solely those of the authors and do not necessarily reflect those of the EPA. EPA does not endorse any products or commercial services mentioned in this publication.

7. References

Bertram, A. K., Martin, S. T., Hanna, S. J., Smith, M. L., Bodsworth, A., Chen, Q., Kuwata, M., Liu, A., You, Y., and Zorn, S. R.: Predicting the relative humidities of liquid-liquid phase separation, efflorescence, and deliquescence of mixed particles of ammonium sulfate, organic material, and water using the organic-to-sulfate mass ratio of the particle and the oxygen-to-carbon elemental ratio of the organic component, Atmos. Chem. Phys., 11, 10995-11006, 10.5194/acp-11-10995-2011, 2011.

727 Blanchard, C. L., Hidy, G. M., Tanenbaum, S., and Edgerton, E. S.: NMOC, ozone, and organic
728 aerosol in the southeastern United States, 1999-2007: 3. Origins of organic aerosol in Atlanta,
729 Georgia, and surrounding areas, Atmospheric Environment, 45, 1291-1302,
730 10.1016/j.atmosenv.2010.12.004, 2011.

731 Blanchard, C. L., Hidy, G. M., Tanenbaum, S., Edgerton, E. S., and Hartsell, B. E.: The
732 Southeastern Aerosol Research and Characterization (SEARCH) study: Temporal trends in gas
733 and PM concentrations and composition, 1999-2010, Journal of the Air & Waste Management
734 Association, 63, 247-259, 10.1080/10962247.2012.748523, 2013a.

735 Blanchard, C. L., Hidy, G. M., Tanenbaum, S., Edgerton, E. S., and Hartsell, B. E.: The
736 Southeastern Aerosol Research and Characterization (SEARCH) study: Spatial variations and
737 chemical climatology, 1999-2010, Journal of the Air & Waste Management Association, 63,
738 260-275, 10.1080/10962247.2012.749816, 2013b.

739 Blanchard, C. L., Tanenbaum, S., and Hidy, G. M.: Source Attribution of Air Pollutant
740 Concentrations and Trends in the Southeastern Aerosol Research and Characterization
741 (SEARCH) Network, Environmental Science & Technology, 47, 13536-13545,
742 10.1021/es402876s, 2013c.

743 Bougiatioti, A., Nikolaou, P., Stavroulas, I., Kouvarakis, G., Weber, R., Nenes, A., Kanakidou,
744 M., and Mihalopoulos, N.: Particle water and pH in the eastern Mediterranean: source variability
745 and implications for nutrient availability, Atmos. Chem. Phys., 16, 4579-4591, 10.5194/acp-16-
746 4579-2016, 2016.

747 Canagaratna, M. R., Jayne, J. T., Jimenez, J. L., Allan, J. D., Alfarra, M. R., Zhang, Q., Onasch,
748 T. B., Drewnick, F., Coe, H., Middlebrook, A., Delia, A., Williams, L. R., Trimborn, A. M.,
749 Northway, M. J., DeCarlo, P. F., Kolb, C. E., Davidovits, P., and Worsnop, D. R.: Chemical and
750 microphysical characterization of ambient aerosols with the aerodyne aerosol mass spectrometer,
751 Mass Spectrometry Reviews, 26, 185-222, 10.1002/mas.20115, 2007.

752 Canagaratna, M. R., Jimenez, J. L., Kroll, J. H., Chen, Q., Kessler, S. H., Massoli, P.,
753 Hildebrandt Ruiz, L., Fortner, E., Williams, L. R., Wilson, K. R., Surratt, J. D., Donahue, N. M.,
754 Jayne, J. T., and Worsnop, D. R.: Elemental ratio measurements of organic compounds using

755 aerosol mass spectrometry: characterization, improved calibration, and implications, Atmos.
756 Chem. Phys., 15, 253-272, 10.5194/acp-15-253-2015, 2015.

757 Case, J. L., and Zavodsky, B. T.: Evolution of 2016 drought in the Southeastern United States
758 from a Land surface modeling perspective, Results in Physics, 8, 654-656,
759 10.1016/j.rinp.2017.12.029, 2018.

760 Chen, J. H., Brooks, C. L., and Scheraga, H. A.: Revisiting the carboxylic acid dimers in aqueous
761 solution: Interplay of hydrogen bonding, hydrophobic interactions, and entropy, Journal of
762 Physical Chemistry B, 112, 242-249, 10.1021/jp074355h, 2008.

763 Clegg, S. L., and Brimblecombe, P.: Equilibrium partial pressures and mean activity and osmotic
764 coefficients of 0-100-percent nitric- acid as a function of temperature, Journal of Physical
765 Chemistry, 94, 5369-5380, 10.1021/j100376a038, 1990.

766 Clegg, S. L., Brimblecombe, P., and Khan, L.: The Henry's law constant of oxalic acid and its
767 partitioning into the atmospheric aerosol, Idojaras, 100, 51-68, 1996.

768 Clegg, S. L., Brimblecombe, P., and Wexler, A. S.: Thermodynamic model of the system H+-
769 NH4+-SO42--NO3--H2O at tropospheric temperatures, Journal of Physical Chemistry A, 102,
770 2137-2154, 10.1021/jp973042r, 1998.

771 DeCarlo, P. F., Kimmel, J. R., Trimborn, A., Northway, M. J., Jayne, J. T., Aiken, A. C., Gonin,
772 M., Fuhrer, K., Horvath, T., Docherty, K. S., Worsnop, D. R., and Jimenez, J. L.: Field-
773 deployable, high-resolution, time-of-flight aerosol mass spectrometer, Analytical Chemistry, 78,
774 8281-8289, 10.1021/ac061249n, 2006.

775 Dentener, F. J., and Crutzen, P. J.: A 3-DIMENSIONAL MODEL OF THE GLOBAL
776 AMMONIA CYCLE, Journal of Atmospheric Chemistry, 19, 331-369, 10.1007/bf00694492,
777 1994.

778 Eatough, D. J., Wadsworth, A., Eatough, D. A., Crawford, J. W., Hansen, L. D., and Lewis, E.
779 A.: A multiple-system, multi-channel diffusion denuder sampler for the determination of fine-
780 particulate organic material in the atmosphere, Atmospheric Environment. Part A. General
781 Topics, 27, 1213-1219, 10.1016/0960-1686(93)90247-V, 1993.

782 Edgerton, E. S., Hartsell, B. E., Saylor, R. D., Jansen, J. J., Hansen, D. A., and Hidy, G. M.: The
783 southeastern aerosol research and characterization study: Part II. Filter-based measurements of
784 fine and coarse particulate matter mass and composition, Journal of the Air & Waste
785 Management Association, 55, 1527-1542, 2005.

786 Edgerton, E. S., Hartsell, B. E., Saylor, R. D., Jansen, J. J., Hansen, D. A., and Hidy, G. M.: The
787 Southeastern Aerosol Research and Characterization Study, part 3: Continuous measurements of
788 fine particulate matter mass and composition, Journal of the Air & Waste Management
789 Association, 56, 1325-1341, 10.1080/10473289.2006.10464585, 2006.

790 Edgerton, E. S., Saylor, R. D., Hartsell, B. E., Jansen, J. J., and Hansen, D. A.: Ammonia and
791 ammonium measurements from the southeastern United States, Atmospheric Environment, 41,
792 3339-3351, 10.1016/j.atmosenv.2006.12.034, 2007.

793 Ellis, R. A., Murphy, J. G., Markovic, M. Z., VandenBoer, T. C., Makar, P. A., Brook, J., and
794 Mihele, C.: The influence of gas-particle partitioning and surface-atmosphere exchange on
795 ammonia during BAQS-Met, Atmos. Chem. Phys., 11, 133-145, 10.5194/acp-11-133-2011,
796 2011.

797 Ellis, R. A., Jacob, D. J., Sulprizio, M. P., Zhang, L., Holmes, C. D., Schichtel, B. A., Blett, T.,
798 Porter, E., Pardo, L. H., and Lynch, J. A.: Present and future nitrogen deposition to national
799 parks in the United States: critical load exceedances, Atmos. Chem. Phys., 13, 9083-9095,
800 10.5194/acp-13-9083-2013, 2013.

801 Ervens, B., Feingold, G., Frost, G. J., and Kreidenweis, S. M.: A modeling study of aqueous
802 production of dicarboxylic acids: 1. Chemical pathways and speciated organic mass production,
803 Journal of Geophysical Research-Atmospheres, 109, 10.1029/2003jd004387, 2004.

804 Fountoukis, C., and Nenes, A.: ISORROPIA II: a computationally efficient thermodynamic
805 equilibrium model for K+-Ca2+-Mg2+-Nh(4)(+)-Na+-SO42--NO3--Cl--H2O aerosols, Atmos.
806 Chem. Phys., 7, 4639-4659, 2007.

807 Gilson, M. K., Given, J. A., Bush, B. L., and McCammon, J. A.: The statistical-thermodynamic
808 basis for computation of binding affinities: A critical review, Biophysical Journal, 72, 1047-
809 1069, 10.1016/s0006-3495(97)78756-3, 1997.

810 Guenther, A. B., Jiang, X., Heald, C. L., Sakulyanontvittaya, T., Duhl, T., Emmons, L. K., and
811 Wang, X.: The Model of Emissions of Gases and Aerosols from Nature version 2.1
812 (MEGAN2.1): an extended and updated framework for modeling biogenic emissions,
813 Geoscientific Model Development, 5, 1471-1492, 10.5194/gmd-5-1471-2012, 2012.

814 Guo, H., Xu, L., Bougiatioti, A., Cerully, K. M., Capps, S. L., Hite, J. R., Jr., Carlton, A. G., Lee,
815 S. H., Bergin, M. H., Ng, N. L., Nenes, A., and Weber, R. J.: Fine-particle water and pH in the
816 southeastern United States, Atmos. Chem. Phys., 15, 5211-5228, 10.5194/acp-15-5211-2015,
817 2015.

818 Guo, H., Sullivan, A. P., Campuzano-Jost, P., Schroder, J. C., Lopez-Hilfiker, F. D., Dibb, J. E.,
819 Jimenez, J. L., Thornton, J. A., Brown, S. S., Nenes, A., and Weber, R. J.: Fine particle pH and
820 the partitioning of nitric acid during winter in the northeastern United States, Journal of
821 Geophysical Research-Atmospheres, 121, 10355-10376, 10.1002/2016jd025311, 2016.

822 Guo, H., Liu, J. M., Froyd, K. D., Roberts, J. M., Veres, P. R., Hayes, P. L., Jimenez, J. L.,
823 Nenes, A., and Weber, R. J.: Fine particle pH and gas-particle phase partitioning of inorganic
824 species in Pasadena, California, during the 2010 CalNex campaign, Atmos. Chem. Phys., 17,
825 5703-5719, 10.5194/acp-17-5703-2017, 2017a.

826 Guo, H., Nenes, A., and Weber, R. J.: The underappreciated role of nonvolatile cations on
827 aerosol ammonium-sulfate molar ratios, Atmos. Chem. Phys. Discuss., 2017, 1-19, 10.5194/acp-
828 2017-737, 2017b.

829 Guo, H., Weber, R. J., and Nenes, A.: High levels of ammonia do not raise fine particle pH
830 sufficiently to yield nitrogen oxide-dominated sulfate production, Scientific Reports, 7,
831 10.1038/s41598-017-11704-0, 2017c.

832 Hansen, D. A., Edgerton, E. S., Hartsell, B. E., Jansen, J. J., Kandasamy, N., Hidy, G. M., and
833 Blanchard, C. L.: The southeastern aerosol research and characterization study: Part 1-overview,
834 Journal of the Air & Waste Management Association, 53, 1460-1471, 2003.

835 Haynes, W. M.: CRC handbook of chemistry and physics: A ready-reference book of chemical
836 and physical data. , Boca Raton: CRC Press, 2014.

837 Hennigan, C. J., Izumi, J., Sullivan, A. P., Weber, R. J., and Nenes, A.: A critical evaluation of
838 proxy methods used to estimate the acidity of atmospheric particles, Atmos. Chem. Phys., 15,
839 2775-2790, 10.5194/acp-15-2775-2015, 2015.

840 Huey, L. G., Hanson, D. R., and Howard, C. J.: Reactions of SF6- and I- with Atmospheric Trace
841 Gases, Journal of Physical Chemistry, 99, 5001-5008, 10.1021/j100014a021, 1995.

842 Huey, L. G., Tanner, D. J., Slusher, D. L., Dibb, J. E., Arimoto, R., Chen, G., Davis, D., Buhr,
843 M. P., Nowak, J. B., Mauldin, R. L., Eisele, F. L., and Kosciuch, E.: CIMS measurements of
844 HNO3 and SO2 at the South Pole during ISCAT 2000, Atmospheric Environment, 38, 5411-
845 5421, 10.1016/j.atmosenv.2004.04.037, 2004.

846 Kawamura, K., and Gagosian, R. B.: Implication of omega-oxocarboxylic acids in the remote
847 marine atmosphere for photo-oxidation of unsaturated fatty acids, Nature, 325, 330-332,
848 10.1038/325330a0, 1987.

849 Kawamura, K., and Ikushima, K.: Seasonal changes in the distribution of dicarboxylic acids in
850 the urban atmosphere, Environmental Science & Technology, 27, 2227-2235,
851 10.1021/es00047a033, 1993.

852 Kawamura, K., and Bikkina, S.: A review of dicarboxylic acids and related compounds in
853 atmospheric aerosols: Molecular distributions, sources and transformation, Atmospheric
854 Research, 170, 140-160, 10.1016/j.atmosres.2015.11.018, 2016.

855 Kerminen, V. M., Ojanen, C., Pakkanen, T., Hillamo, R., Aurela, M., and Merilainen, J.: Low-
856 molecular-weight dicarboxylic acids in an urban and rural atmosphere, Journal of Aerosol
857 Science, 31, 349-362, 10.1016/s0021-8502(99)00063-4, 2000.

858 Laskin, A., Laskin, J., and Nizkorodov, S. A.: Chemistry of Atmospheric Brown Carbon,
859 Chemical Reviews, 115, 4335-4382, 10.1021/cr5006167, 2015.

860 Laskin, J., Laskin, A., Roach, P. J., Slysz, G. W., Anderson, G. A., Nizkorodov, S. A., Bones, D.
861 L., and Nguyen, L. Q.: High-Resolution Desorption Electrospray Ionization Mass Spectrometry
862 for Chemical Characterization of Organic Aerosols, Analytical Chemistry, 82, 2048-2058,
863 10.1021/ac902801f, 2010.

864 Lee, H. J., Laskin, A., Laskin, J., and Nizkorodov, S. A.: Excitation-Emission Spectra and
865 Fluorescence Quantum Yields for Fresh and Aged Biogenic Secondary Organic Aerosols,
866 Environmental Science & Technology, 47, 5763-5770, 10.1021/es400644c, 2013.

867 Lim, H. J., Carlton, A. G., and Turpin, B. J.: Isoprene forms secondary organic aerosol through
868 cloud processing: Model simulations, Environmental Science & Technology, 39, 4441-4446,
869 10.1021/es048039h, 2005.

870 Liu, J., Zhang, X., Parker, E. T., Veres, P. R., Roberts, J. M., de Gouw, J. A., Hayes, P. L.,
871 Jimenez, J. L., Murphy, J. G., Ellis, R. A., Huey, L. G., and Weber, R. J.: On the gas-particle
872 partitioning of soluble organic aerosol in two urban atmospheres with contrasting emissions: 2.
873 Gas and particle phase formic acid, Journal of Geophysical Research-Atmospheres, 117,
874 10.1029/2012jd017912, 2012.

875 Malm, W. C., and Day, D. E.: Estimates of aerosol species scattering characteristics as a function
876 of relative humidity, Atmospheric Environment, 35, 2845-2860, 10.1016/s1352-2310(01)00077-
877 2, 2001.

878 Middlebrook, A. M., Bahreini, R., Jimenez, J. L., and Canagaratna, M. R.: Evaluation of
879 Composition-Dependent Collection Efficiencies for the Aerodyne Aerosol Mass Spectrometer
880 using Field Data, Aerosol Science and Technology, 46, 258-271,
881 10.1080/02786826.2011.620041, 2012.

882 Na, K., Song, C., Switzer, C., and Cocker, D. R.: Effect of ammonia on secondary organic
883 aerosol formation from alpha-Pinene ozonolysis in dry and humid conditions, Environmental
884 Science & Technology, 41, 6096-6102, 10.1021/es061956y, 2007.

885 Nah, T., Ji, Y., Tanner, D. J., Guo, H., Sullivan, A. P., Ng, N. L., Weber, R. J., and Huey, L. G.:
886 Real-time measurements of gas-phase organic acids using SF6- chemical ionization mass
887 spectrometry, Atmos. Meas. Tech. Discuss., 2018, 1-40, 10.5194/amt-2018-46, 2018.

888 Nenes, A., Pandis, S. N., and Pilinis, C.: ISORROPIA: A new thermodynamic equilibrium model
889 for multiphase multicomponent inorganic aerosols, Aquatic Geochemistry, 4, 123-152,
890 10.1023/a:1009604003981, 1998.

891 Neuman, J. A., Ryerson, T. B., Huey, L. G., Jakoubek, R., Nowak, J. B., Simons, C., and
892 Fehsenfeld, F. C.: Calibration and evaluation of nitric acid and ammonia permeation tubes by
893 UV optical absorption, Environmental Science & Technology, 37, 2975-2981,
894 10.1021/es0264221, 2003.

895 Nowak, J. B., Huey, L. G., Eisele, F. L., Tanner, D. J., Mauldin, R. L., Cantrell, C., Kosciuch, E.,
896 and Davis, D. D.: Chemical ionization mass spectrometry technique for detection of
897 dimethylsulfoxide and ammonia, Journal of Geophysical Research-Atmospheres, 107,
898 10.1029/2001jd001058, 2002.

899 Nowak, J. B., Huey, L. G., Russell, A. G., Tian, D., Neuman, J. A., Orsini, D., Sjostedt, S. J.,
900 Sullivan, A. P., Tanner, D. J., Weber, R. J., Nenes, A., Edgerton, E., and Fehsenfeld, F. C.:
901 Analysis of urban gas phase ammonia measurements from the 2002 Atlanta Aerosol Nucleation
902 and Real-Time Characterization Experiment (ANARChE), Journal of Geophysical Research-
903 Atmospheres, 111, 14, 10.1029/2006jd007113, 2006.

904 Orsini, D. A., Ma, Y. L., Sullivan, A., Sierau, B., Baumann, K., and Weber, R. J.: Refinements to
905 the particle-into-liquid sampler (PILS) for ground and airborne measurements of water soluble
906 aerosol composition, Atmospheric Environment, 37, 1243-1259, 10.1016/s1352-2310(02)01015-
907 4, 2003.

908 Park Williams, A., Cook, B. I., Smerdon, J. E., Bishop, D. A., Seager, R., and Mankin, J. S.: The
909 2016 Southeastern U.S. Drought: An Extreme Departure From Centennial Wetting and Cooling,
910 Journal of Geophysical Research: Atmospheres, 122, 10,888-810,905, 10.1002/2017JD027523,
911 2017.

912 Pechony, O., and Shindell, D. T.: Driving forces of global wildfires over the past millennium and
913 the forthcoming century, Proceedings of the National Academy of Sciences of the United States
914 of America, 107, 19167-19170, 10.1073/pnas.1003669107, 2010.

915 Reis, S., Pinder, R. W., Zhang, M., Lijie, G., and Sutton, M. A.: Reactive nitrogen in
916 atmospheric emission inventories, Atmos. Chem. Phys., 9, 7657-7677, 10.5194/acp-9-7657-
917 2009, 2009.

918 Sander, R.: Compilation of Henry's law constants (version 4.0) for water as solvent, Atmos.
919 Chem. Phys., 15, 4399-4981, 10.5194/acp-15-4399-2015, 2015.

920 Saxena, P., and Hildemann, L. M.: Water-soluble organics in atmospheric particles: A critical
921 review of the literature and application of thermodynamics to identify candidate compounds,
922 Journal of Atmospheric Chemistry, 24, 57-109, 10.1007/bf00053823, 1996.

923 Saylor, R., Myles, L., Sibble, D., Caldwell, J., and Xing, J.: Recent trends in gas-phase ammonia
924 and PM2.5 ammonium in the Southeast United States, Journal of the Air & Waste Management
925 Association, 65, 347-357, 10.1080/10962247.2014.992554, 2015.

926 Schrier, E. E., Pottle, M., and Scheraga, H. A.: The Influence of Hydrogen and Hydrophobic
927 Bonds on the Stability of the Carboxylic Acid Dimers in Aqueous Solution, Journal of the
928 American Chemical Society, 86, 3444-3449, 10.1021/ja01071a009, 1964.

929 Seinfeld, J. H., and Pandis, S. N.: Atmospheric chemistry and physics : from air pollution to
930 climate change, Third edition. ed., John Wiley & Sons, Inc., Hoboken, New Jersey, xxvi, 1120
931 pages pp., 2016.

932 Shi, G. L., Xu, J., Peng, X., Xiao, Z. M., Chen, K., Tian, Y. Z., Guan, X. B., Feng, Y. C., Yu, H.
933 F., Nenes, A., and Russell, A. G.: pH of Aerosols in a Polluted Atmosphere: Source
934 Contributions to Highly Acidic Aerosol, Environmental Science & Technology, 51, 4289-4296,
935 10.1021/acs.est.6b05736, 2017.

936 Song, M., Marcolli, C., Krieger, U. K., Zuend, A., and Peter, T.: Liquid-liquid phase separation
937 and morphology of internally mixed dicarboxylic acids/ammonium sulfate/water particles,
938 Atmos. Chem. Phys., 12, 2691-2712, 10.5194/acp-12-2691-2012, 2012.

939 Song, S., Gao, M., Xu, W., Shao, J., Shi, G., Wang, S., Wang, Y., Sun, Y., and McElroy, M. B.:
940 Fine particle pH for Beijing winter haze as inferred from different thermodynamic equilibrium
941 models, Atmos. Chem. Phys. Discuss., 2018, 1-26, 10.5194/acp-2018-6, 2018.

942 Sorooshian, A., Ng, N. L., Chan, A. W. H., Feingold, G., Flagan, R. C., and Seinfeld, J. H.:
943 Particulate organic acids and overall water-soluble aerosol composition measurements from the
944 2006 Gulf of Mexico Atmospheric Composition and Climate Study (GoMACCS), Journal of
945 Geophysical Research-Atmospheres, 112, 16, 10.1029/2007jd008537, 2007.

946 Sorooshian, A., Murphy, S. M., Hersey, S., Bahreini, R., Jonsson, H., Flagan, R. C., and
947 Seinfeld, J. H.: Constraining the contribution of organic acids and AMS m/z 44 to the organic
948 aerosol budget: On the importance of meteorology, aerosol hygroscopicity, and region,
949 Geophysical Research Letters, 37, 5, 10.1029/2010gl044951, 2010.

950 Spaulding, R. S., Talbot, R. W., and Charles, M. J.: Optimization of a mist chamber (cofer
951 scrubber) for sampling water-soluble organics in air, Environmental Science & Technology, 36,
952 1798-1808, 10.1021/es011189x, 2002.

953 Sullivan, A. P., Weber, R. J., Clements, A. L., Turner, J. R., Bae, M. S., and Schauer, J. J.: A
954 method for on-line measurement of water-soluble organic carbon in ambient aerosol particles:
955 Results from an urban site, Geophysical Research Letters, 31, 10.1029/2004gl019681, 2004.

956 Sun, K., Tao, L., Miller, D. J., Pan, D., Golston, L. M., Zondlo, M. A., Griffin, R. J., Wallace, H.
957 W., Leong, Y. J., Yang, M. M., Zhang, Y., Mauzerall, D. L., and Zhu, T.: Vehicle Emissions as
958 an Important Urban Ammonia Source in the United States and China, Environmental Science &
959 Technology, 51, 2472-2481, 10.1021/acs.est.6b02805, 2017.

960 Updyke, K. M., Nguyen, T. B., and Nizkorodov, S. A.: Formation of brown carbon via reactions
961 of ammonia with secondary organic aerosols from biogenic and anthropogenic precursors,
962 Atmospheric Environment, 63, 22-31, 10.1016/j.atmosenv.2012.09.012, 2012.

963 Van Damme, M., Clarisse, L., Heald, C. L., Hurtmans, D., Ngadi, Y., Clerbaux, C., Dolman, A.
964 J., Erisman, J. W., and Coheur, P. F.: Global distributions, time series and error characterization

965 of atmospheric ammonia (NH3) from IASI satellite observations, Atmos. Chem. Phys., 14, 2905-
966 2922, 10.5194/acp-14-2905-2014, 2014.

967 Warner, J. X., Wei, Z. G., Strow, L. L., Dickerson, R. R., and Nowak, J. B.: The global
968 tropospheric ammonia distribution as seen in the 13-year AIRS measurement record, Atmos.
969 Chem. Phys., 16, 5467-5479, 10.5194/acp-16-5467-2016, 2016.

970 Warner, J. X., Dickerson, R. R., Wei, Z., Strow, L. L., Wang, Y., and Liang, Q.: Increased
971 atmospheric ammonia over the world's major agricultural areas detected from space, Geophysical
972 Research Letters, 44, 2875-2884, 10.1002/2016gl072305, 2017.

973 Weber, R. J., Orsini, D., Daun, Y., Lee, Y. N., Klotz, P. J., and Brechtel, F.: A particle-into-
974 liquid collector for rapid measurement of aerosol bulk chemical composition, Aerosol Science
975 and Technology, 35, 718-727, 10.1080/02786820152546761, 2001.

976 Weber, R. J., Lee, S., Chen, G., Wang, B., Kapustin, V., Moore, K., Clarke, A. D., Mauldin, L.,
977 Kosciuch, E., Cantrell, C., Eisele, F., Thornton, D. C., Bandy, A. R., Sachse, G. W., and
978 Fuelberg, H. E.: New particle formation in anthropogenic plumes advecting from Asia observed
979 during TRACE-P, Journal of Geophysical Research-Atmospheres, 108, 13,
980 10.1029/2002jd003112, 2003.

981 Weber, R. J., Guo, H., Russell, A. G., and Nenes, A.: High aerosol acidity despite declining
982 atmospheric sulfate concentrations over the past 15 years, Nature Geoscience, 9, 282-+,
983 10.1038/ngeo2665, 2016.

984 Xing, J., Pleim, J., Mathur, R., Pouliot, G., Hogrefe, C., Gan, C. M., and Wei, C.: Historical
985 gaseous and primary aerosol emissions in the United States from 1990 to 2010, Atmos. Chem.
986 Phys., 13, 7531-7549, 10.5194/acp-13-7531-2013, 2013.

987 Xu, L., Guo, H., Boyd, C. M., Klein, M., Bougiatioti, A., Cerully, K. M., Hite, J. R., Isaacman-
988 VanWertz, G., Kreisberg, N. M., Knote, C., Olson, K., Koss, A., Goldstein, A. H., Hering, S. V.,
989 de Gouw, J., Baumann, K., Lee, S.-H., Nenes, A., Weber, R. J., and Ng, N. L.: Effects of
990 anthropogenic emissions on aerosol formation from isoprene and monoterpenes in the

991 southeastern United States, Proceedings of the National Academy of Sciences of the United
992 States of America, 112, 37-42, 10.1073/pnas.1417609112, 2015a.

993 Xu, L., Suresh, S., Guo, H., Weber, R. J., and Ng, N. L.: Aerosol characterization over the
994 southeastern United States using high-resolution aerosol mass spectrometry: spatial and seasonal
995 variation of aerosol composition and sources with a focus on organic nitrates, Atmos. Chem.
996 Phys., 15, 7307-7336, 10.5194/acp-15-7307-2015, 2015b.

997 Xu, L., Guo, H. Y., Weber, R. J., and Ng, N. L.: Chemical Characterization of Water-Soluble
998 Organic Aerosol in Contrasting Rural and Urban Environments in the Southeastern United
999 States, Environmental Science & Technology, 51, 78-88, 10.1021/acs.est.6b05002, 2017.

1000 Yao, X. H., Hu, Q. J., Zhang, L. M., Evans, G. J., Godri, K. J., and Ng, A. C.: Is vehicular
1001 emission a significant contributor to ammonia in the urban atmosphere?, Atmospheric
1002 Environment, 80, 499-506, 10.1016/j.atmosenv.2013.08.028, 2013.

1003 You, Y., Renbaum-Wolff, L., and Bertram, A. K.: Liquid-liquid phase separation in particles
1004 containing organics mixed with ammonium sulfate, ammonium bisulfate, ammonium nitrate or
1005 sodium chloride, Atmos. Chem. Phys., 13, 11723-11734, 10.5194/acp-13-11723-2013, 2013.

1006 You, Y., Kanawade, V. P., de Gouw, J. A., Guenther, A. B., Madronich, S., Sierra-Hernandez,
1007 M. R., Lawler, M., Smith, J. N., Takahama, S., Ruggeri, G., Koss, A., Olson, K., Baumann, K.,
1008 Weber, R. J., Nenes, A., Guo, H., Edgerton, E. S., Porcelli, L., Brune, W. H., Goldstein, A. H.,
1009 and Lee, S. H.: Atmospheric amines and ammonia measured with a chemical ionization mass
1010 spectrometer (CIMS), Atmos. Chem. Phys., 14, 12181-12194, 10.5194/acp-14-12181-2014,
1011 2014a.

1012 You, Y., Smith, M. L., Song, M., Martin, S. T., and Bertram, A. K.: Liquid-liquid phase
1013 separation in atmospherically relevant particles consisting of organic species and inorganic salts,
1014 International Reviews in Physical Chemistry, 33, 43-77, 10.1080/0144235x.2014.890786, 2014b.

1015 You, Y., and Bertram, A. K.: Effects of molecular weight and temperature on liquid-liquid phase
1016 separation in particles containing organic species and inorganic salts, Atmos. Chem. Phys., 15,
1017 1351-1365, 10.5194/acp-15-1351-2015, 2015.

1018 Yu, H., and Lee, S. H.: Chemical ionisation mass spectrometry for the measurement of
1019 atmospheric amines, Environ. Chem., 9, 190-201, 10.1071/en12020, 2012.

1020 Zuend, A., Marcolli, C., Luo, B. P., and Peter, T.: A thermodynamic model of mixed organic-
1021 inorganic aerosols to predict activity coefficients, Atmos. Chem. Phys., 8, 4559-4593,
1022 10.5194/acp-8-4559-2008, 2008.

1023 Zuend, A., Marcolli, C., Booth, A. M., Lienhard, D. M., Soonsin, V., Krieger, U. K., Topping, D.
1024 O., McFiggans, G., Peter, T., and Seinfeld, J. H.: New and extended parameterization of the
1025 thermodynamic model AIOMFAC: calculation of activity coefficients for organic-inorganic
1026 mixtures containing carboxyl, hydroxyl, carbonyl, ether, ester, alkenyl, alkyl, and aromatic
1027 functional groups, Atmos. Chem. Phys., 11, 9155-9206, 10.5194/acp-11-9155-2011, 2011.

1028 Zuend, A., Marcolli, C., Luo, B. P., and Peter, T.: A thermodynamic model of mixed organic-
1029 inorganic aerosols to predict activity coefficients (vol 8, pg 4559, 2008), Atmos. Chem. Phys.,
1030 12, 10075-10075, 10.5194/acp-12-10075-2012, 2012.
1031

1032

1033

1034

1035

1036

1037

1038

1039

1040

1041

Atmos. Chem. Phys. Discuss., https://doi.org/10.5194/acp-2018-373
Manuscript under review for journal Atmos. Chem. Phys.
Discussion started: 26 April 2018

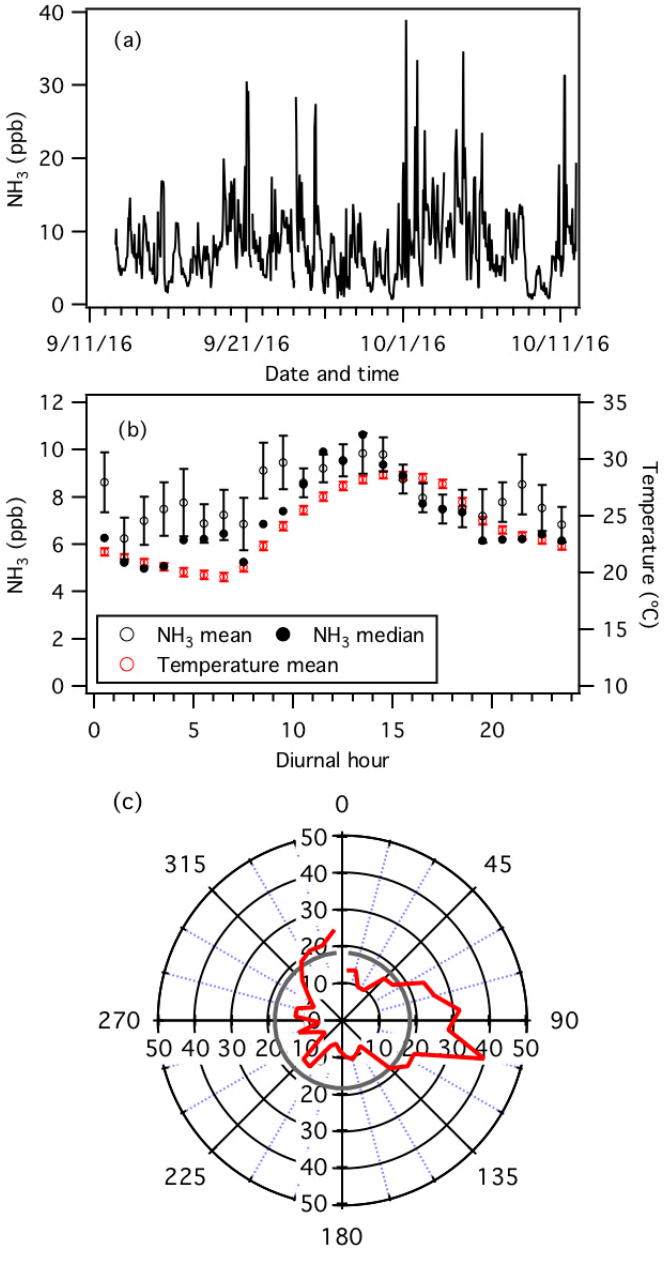

1042

1043 **Figure 1:** Measurements by the NH_3-CIMS during the second half of the study. (a) Time series
1044 of NH_3 concentration. The data is displayed as 1-hour averages. (b) Diurnal profiles of NH_3
1045 concentration (mean and median) and temperature. Error bars shown are the standard errors.
1046 Dates and times displayed are local time. All the concentrations represent averages in 1-hour

1047 intervals and the standard errors are plotted as error bars. (c) Average NH_3 concentration
1048 normalized to wind speed (i.e., NH_3 concentration (ppb) x wind speed (m s^{-1})) in each 10 degrees
1049 bin (red line). The study-averaged normalized NH_3 concentration is shown as a grey line.

1050

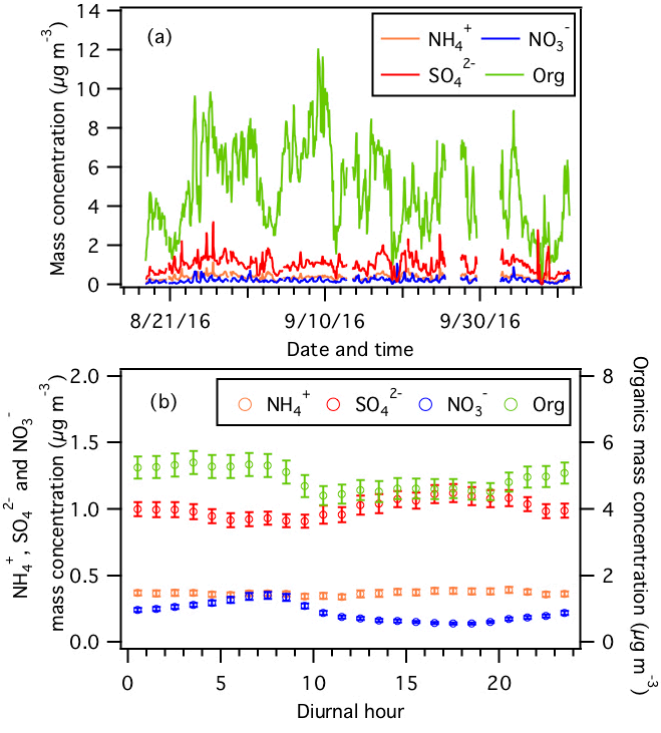

1051

1052 **Figure 2:** (a) Time series and (b) diurnal profiles of non-refractory PM_1 species measured by the
1053 AMS. Error bars shown in panel (b) are the standard errors. Dates and times displayed are local
1054 time. All the mass concentrations shown here are obtained from scaling the raw data by 0.5.
1055 Refer to the text for details.

Atmos. Chem. Phys. Discuss., https://doi.org/10.5194/acp-2018-373
Manuscript under review for journal Atmos. Chem. Phys.
Discussion started: 26 April 2018

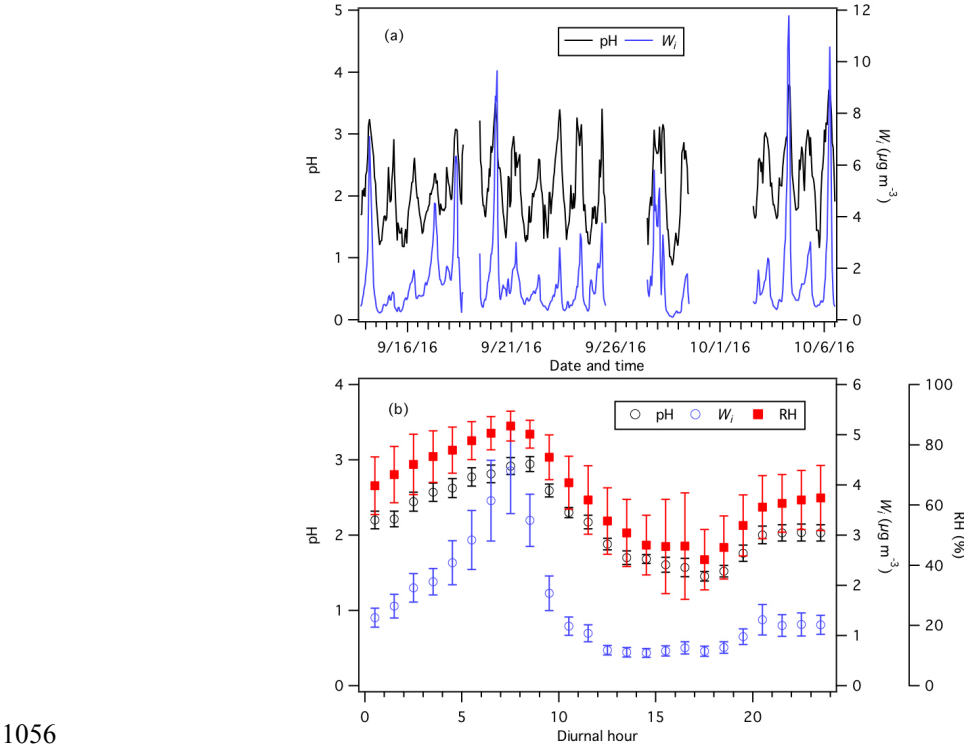

Figure 3: (a) Time series and (b) diurnal profiles of ISORROPIA-predicted PM_1 pH and W_i. Dates and times displayed are local time. All the data shown here represent averages in 1-hour intervals. Error bars shown in panel (b) are the standard errors.

Atmos. Chem. Phys. Discuss., https://doi.org/10.5194/acp-2018-373
Manuscript under review for journal Atmos. Chem. Phys.
Discussion started: 26 April 2018

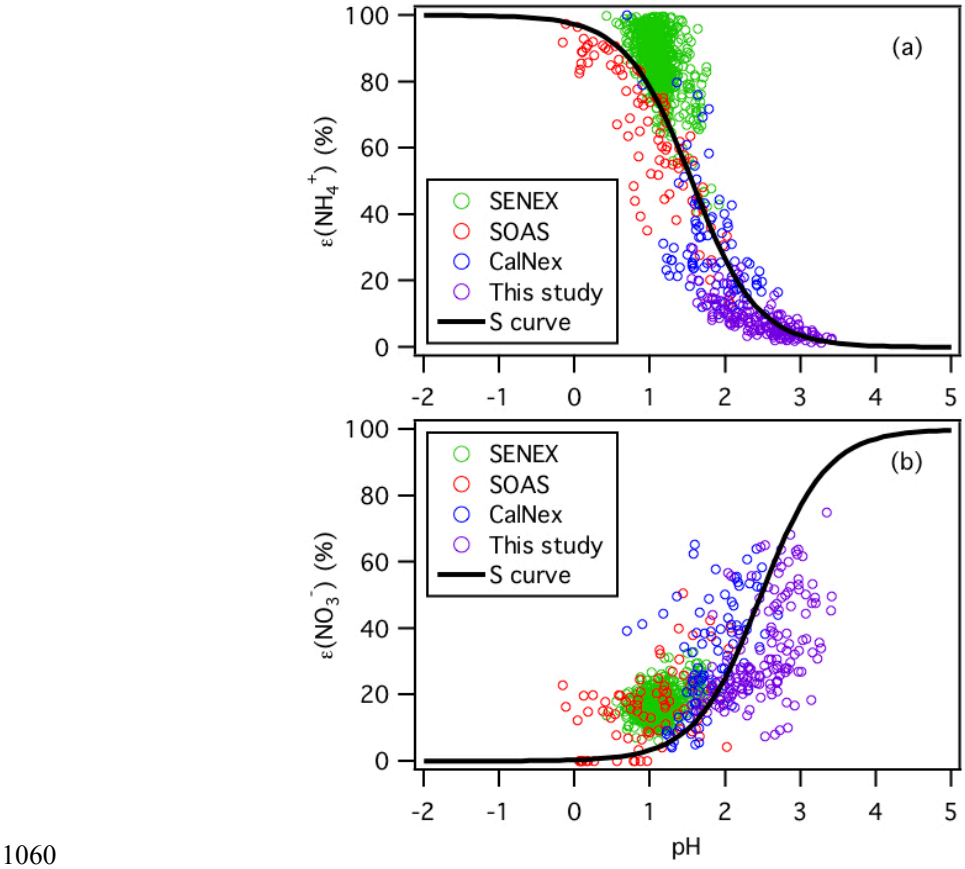

1060

1061 **Figure 4:** Analytically calculated S curves of $\varepsilon(NH_4^+)$ and $\varepsilon(NO_3^-)$ and ambient data plotted
1062 against ISORROPIA-predicted particle pH for this study, SENEX, SOAS and CalNex. For the
1063 ambient datasets, a narrow range of W_i (1 to 4 μg m^{-3}) and temperature (15 to 25 °C) are selected
1064 to be close to the analytical calculation input (i.e., W_i = 2.5 μg m^{-3} and temperature = 20 °C).
1065 Similar to Guo et al. (2017a), $\gamma_{NH_4^+} = 1$ and $\gamma_{H^+-NO_3^-} = \sqrt{\gamma_{H^+}\gamma_{NO_3^-}} = 0.28$ are used for the
1066 analytically calculated S curves.

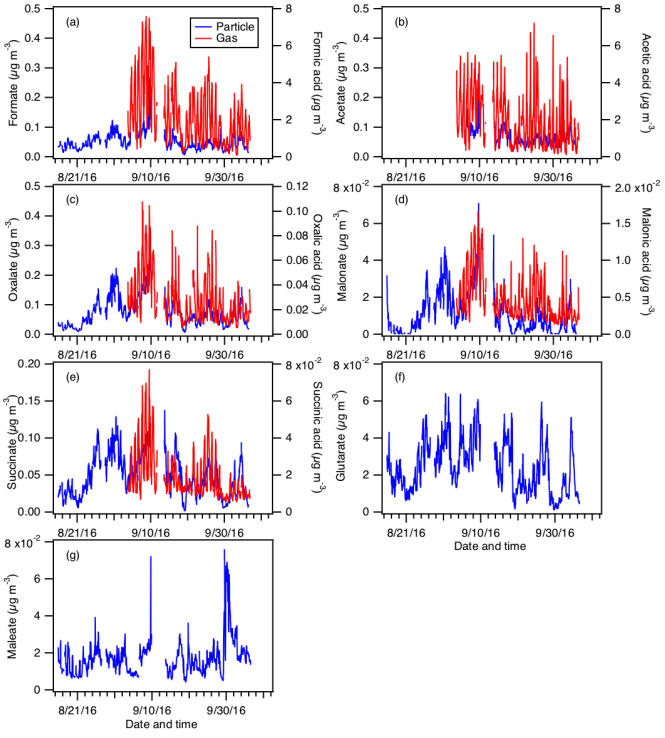

1067

1068 **Figure 5:** Particle- and gas-phase measurements of (a) formic, (b) acetic, (c) oxalic, (d) malonic,
1069 (e) succinic, (f) glutaric, and (g) maleic acids. Particle-phase measurements are shown on the left
1070 y axes, while gas-phase measurements are shown on the right y axes. Dates and times displayed
1071 are local time. Gas-phase measurements of glutaric and maleic acids are not available.

Atmos. Chem. Phys. Discuss., https://doi.org/10.5194/acp-2018-373
Manuscript under review for journal Atmos. Chem. Phys.
Discussion started: 26 April 2018

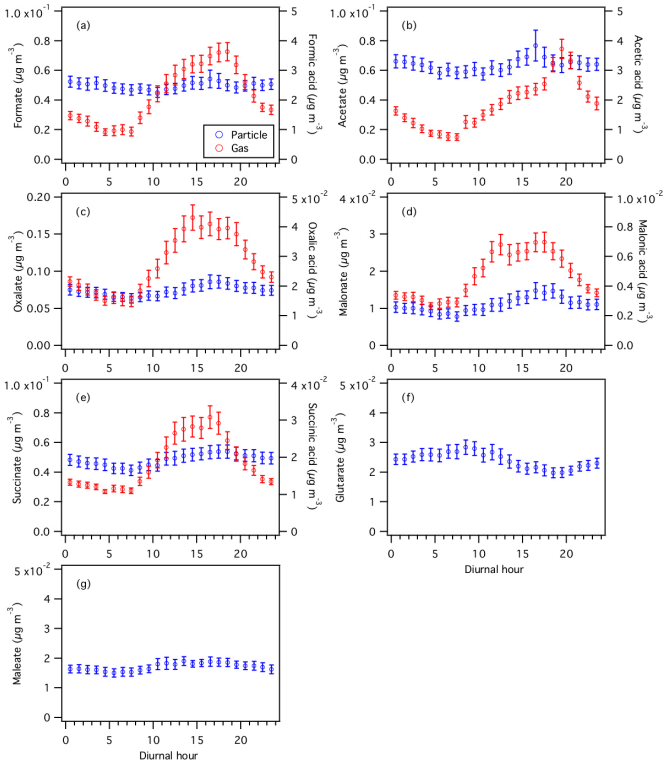

1072

1073 **Figure 6:** Diurnal profiles of particle- and gas-phase (a) formic, (b) acetic, (c) oxalic, (d)
1074 malonic, (e) succinic, (f) glutaric, and (g) maleic acids. Particle-phase measurements are shown
1075 on the left y axes, while gas-phase measurements are shown on the right y axes. All the data
1076 shown here represent averages in 1-hour intervals. Error bars shown are the standard errors.

1077

1078

Atmos. Chem. Phys. Discuss., https://doi.org/10.5194/acp-2018-373
Manuscript under review for journal Atmos. Chem. Phys.
Discussion started: 26 April 2018

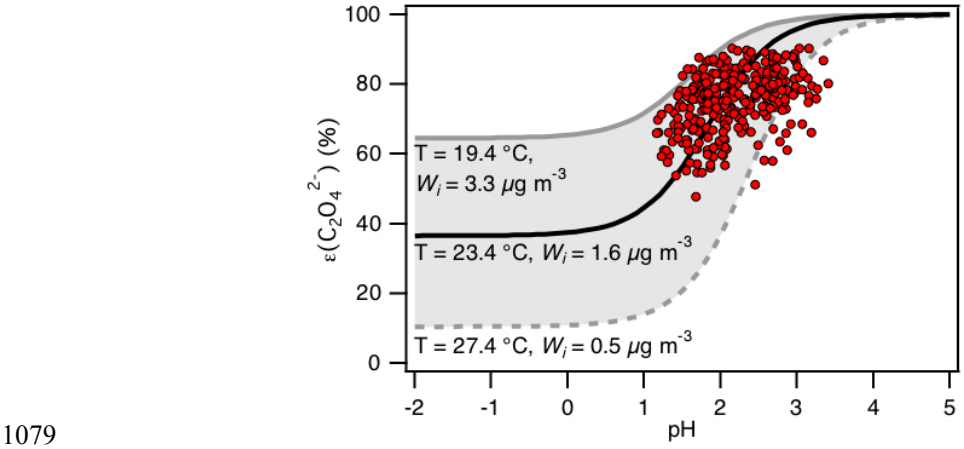

Figure 7: Analytically calculated S curve of $\varepsilon(C_2O_4^{2-})$ and ambient data from 13 September to 6 October 2016 plotted against ISORROPIA-predicted particle pH. For the ambient data, a range in W_i (0.5 to 4 μg m^{-3}) and temperature (15 to 31 °C) are chosen to be close to the analytically calculated outputs. For the analytically calculated S curves, we used $\gamma_{C_2H_2O_4}$ = 0.0492 (AIOMFAC predicted). We also assumed that $\gamma_{H^+}\gamma_{C_2HO_4^-} = \gamma_{H^+}\gamma_{NO_3^-}$, and used the ISORROPIA-predicted $\gamma_{H^+-NO_3^-} = \sqrt{\gamma_{H^+}\gamma_{NO_3^-}}$ = 0.265. The black line is the S curve calculated using the selected time period's average temperature (23.4 ± 4.0 °C) and W_i (1.6 ± 1.7 μg m^{-3}). The grey lines are S curves calculated using one standard deviation from the average temperature and W_i (i.e., temperature = 27.4 °C and W_i = 0.5 μg m^{-3} for dotted grey line, temperature = 19.4 °C and W_i = 3.3 μg m^{-3} for solid grey line).

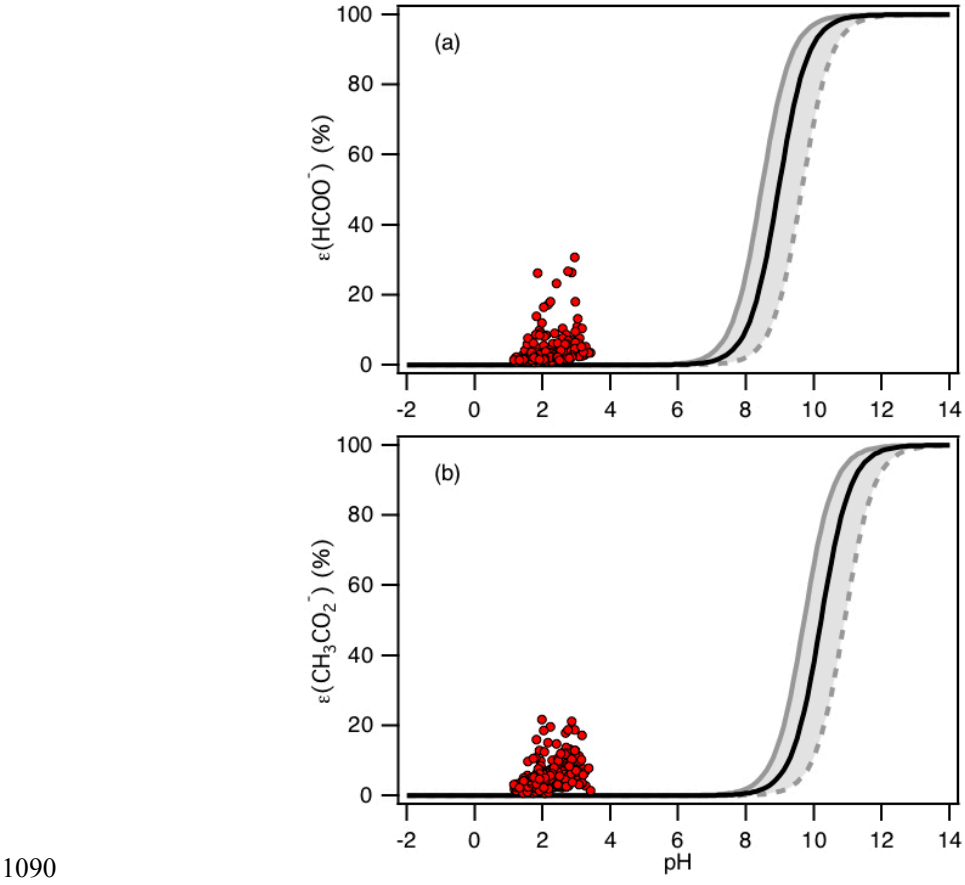

Figure 8: Analytically calculated S curves of ε($HCOO^-$) and ε($CH_3CO_2^-$) (solid black lines) and ambient data from 13 September to 6 October 2016 plotted against ISORROPIA-predicted particle pH (shown in panels (a) and (b), respectively). For the ambient data, a narrow range in W_i (0.5 to 4 μg m^{-3}) and RH (20 to 90 %) is chosen to be close to the analytically calculated outputs. For the analytically calculated S curves, we used γ_{HCOOH} = 0.334 and γ_{CH_3COOH} = 2.150 (AIOMFAC predicted). We also assumed that $\gamma_{H^+}\gamma_{HCOO^-} = \gamma_{H^+}\gamma_{CH_3COO^-} = \gamma_{H^+}\gamma_{NO_3^-}$, and used the ISORROPIA-predicted $\gamma_{H^+-NO_3^-} = \sqrt{\gamma_{H^+}\gamma_{NO_3^-}}$ = 0.265. The black lines are S curves calculated using the selected time period's average temperature (23.4 ± 4.0 °C) and W_i (1.6 ± 1.7 μg m^{-3}). The grey lines are S curves calculated using one standard deviation from the average temperature and W_i (i.e., temperature = 27.4 °C and W_i = 0.5 μg m^{-3} for dotted grey line, temperature = 19.4 °C and W_i = 3.3 μg m^{-3} for solid grey line).

Table 1: Comparisons between different field campaigns for particle pH, major inorganic ions and gases and meteorological conditions. All pH values were calculated using ISORROPIA-II run in forward mode. These statistics were previously compiled by Guo et al. (2017a). Campaign acronyms used here stand for the California Research at the Nexus of Air Quality and Climate Change (CalNex), Southern Oxidant and Aerosol Study (SOAS), and Southeastern Nexus of Air Quality and Climate (SENEX).

Campaign	CalNex		SOAS	SENEX	This study
Type	Ground		Ground	Aircraft	Ground
PM cut size	PM_1	$PM_{2.5}$[a]	PM_1&$PM_{2.5}$[b]	PM_1	PM_1
Year	2010		2013	2013	2016
Season	(Early Summer)		Summer	Summer	Fall
Region/Location	SW US		SE US	SE US	SE US
SO_4^{2-}, μg m^{-3}	2.86 ± 1.70	1.88 ± 0.69	1.73 ± 1.21	2.05 ± 0.80	1.6 ± 0.4
NO_3^-, μg m^{-3}	3.58 ± 3.65	3.74 ± 1.53	0.08 ± 0.08	0.28 ± 0.09	0.20 ± 0.10
HNO_3, μg m^{-3}	6.65 ± 7.03	4.45 ± 3.59	0.36 ± 0.14	1.35 ± 0.66	0.50 ± 0.26
ε(NO_3^-)	39 ± 16 %	51 ± 18 %	22 ± 16 %	18 ± 6 %	26 ± 15 %
Total NO_3^-, μg m^{-3}	10.22 ± 9.74	8.19 ± 3.89	0.45 ± 0.26	1.63 ± 0.70	0.70 ± 0.28
NH_4^+, μg m^{-3}	2.06 ± 1.67	1.79 ± 0.65	0.46 ± 0.34	1.06 ± 0.25	0.40 ± 0.20
NH_3, μg m^{-3}	1.37 ± 0.90	0.75 ± 0.61	0.39 ± 0.25	0.12 ± 0.19	5.79 ± 3.67
ε(NH_4^+)	55 ± 25%	71 ± 19%	50 ± 25%	92 ± 11%	7 ± 5 %
Total NH_4^+, μg m^{-3}	3.44 ± 1.81	2.54 ± 0.89	0.78 ± 0.50	1.17 ± 0.81	6.19 ± 3.68
Na^+, μg m^{-3}	\	0.77 ± 0.39	0.03 ± 0.07	\	\
Cl^-, μgm^{-3}	\	0.64 ± 0.48	0.02 ± 0.03	\	0.01 ± 0.01
RH, %	79 ± 17	87 ± 9	74 ± 16	72 ± 9	69 ± 18
T, °C	18 ± 4	18 ± 3	25 ± 3	22 ± 3	24 ± 4
W_i, μg m^{-3}	13.9 ± 18.1	29.8 ± 20.7	5.1 ± 3.8	3.2 ± 2.8	1.6 ± 1.7
pH	1.9 ± 0.5	2.7 ± 0.3	0.9 ± 0.6	1.1 ± 0.4	2.2 ± 0.6
Reference	(Guo et al., 2017a)		(Guo et al., 2015)	(Xu et al., 2016)	This study

[a]Only during the last week of CalNex.

[b]$PM_{2.5}$ was sampled in the first half and PM_1 sampled in the second half of the study. Various parameters were similar in both cases. Crustal components were higher, but are overall generally in low concentrations so the differences had minor effects. For example, $PM_{2.5}$ Na^+ was 0.06 ± 0.09 μg m^{-3} and PM_1 Na^+ was 0.01 ± 0.01 μg m^{-3}.